Adult somatic progenitor cells and hematopoiesis in oysters

M. Jemaa, N. Morin, P. Cavelier, J. Cau, Jm Strub, C. Delsert

© 2014. Published by The Company of Biologists Ltd | The Journal of Experimental Biology (2014) 217, 3067-3077 doi:10.1242/jeb.106575

RESEARCH ARTICLE

Adult somatic progenitor cells and hematopoiesis in oysters

Mohamed Jemaà[1,2], Nathalie Morin[1,2], Patricia Cavelier[1,3], Julien Cau[1,4], Jean Marc Strub[5,6] and Claude Delsert[1,2,7,*]

ABSTRACT

Long-lived animals show a non-observable age-related decline in immune defense, which is provided by blood cells that derive from self-renewing stem cells. The oldest living animals are bivalves. Yet, the origin of hemocytes, the cells involved in innate immunity, is unknown in bivalves and current knowledge about mollusk adult somatic stem cells is scarce. Here we identify a population of adult somatic precursor cells and show their differentiation into hemocytes. Oyster gill contains an as yet unreported irregularly folded structure (IFS) with stem-like cells bathing into the hemolymph. BrdU labeling revealed that the stem-like cells in the gill epithelium and in the nearby hemolymph replicate DNA. Proliferation of this cell population was further evidenced by phosphorylated-histone H3 mitotic staining. Finally, these small cells, most abundant in the IFS epithelium, were found to be positive for the stemness marker Sox2. We provide evidence for hematopoiesis by showing that co-expression of Sox2 and Cu/Zn superoxide dismutase, a hemocyte-specific enzyme, does not occur in the gill epithelial cells but rather in the underlying tissues and vessels. We further confirm the hematopoietic features of these cells by the detection of Filamin, a protein specific for a sub-population of hemocytes, in large BrdU-labeled cells bathing into gill vessels. Altogether, our data show that progenitor cells differentiate into hemocytes in the gill, which suggests that hematopoiesis occurs in oyster gills.

KEY WORDS: Hematopoiesis, Adult somatic progenitor cells, Hemocytes, Mollusk, Marine invertebrates

INTRODUCTION

The longest living animals belong to the Bivalvia (Bureau et al., 2002; Peck and Bullough, 1993; Turekian et al., 1975; Ziuganov et al., 2000; Wanamaker et al., 2008; Butler et al., 2013), a main class in the phylum Mollusca. Long-lived animals have been defined as non-senescing species (Finch and Austad, 2001) because they do not show any observable age-related decline in physiological capacity or disease resistance. Indeed, bivalves grow and, most importantly, they ensure their immune defense during their entire life (Bodnar, 2009). In bivalves, immunity involves both cell-mediated and humoral systems that operate in a coordinated way (for reviews, see Pruzzo et al., 2005; Schmitt et al., 2012). The cell-mediated immune defense is carried out by blood cells that are continuously produced in the adult animal and that derive from self-renewing populations of multipotent stem cells that are housed in specialized hematopoeitic organs (reviewed in Hartenstein, 2006). Yet, the origin of blood cells is unknown in bivalves (Vogt, 2012). Moreover, our current knowledge about mollusk adult somatic stem cells is scarce. Mollusk cellular immunity is ensured by motile hemocytes (Cheng, 1996) circulating through the hemolymph before infiltrating tissues (Galtsoff, 1964; Eble and Scro, 1996). Three main types of hemocytes have been recognized in mollusks based upon their morphology: (1) granular cells with numerous cytoplasmic granulations, (2) hyaline cells with a clear cytoplasm and (3) rare and much smaller stem-like cells (Hartenstein, 2006; Cheng, 1996; Kuchel et al., 2011).

Despite a long-standing interest in the bivalve immune system (Cuénot, 1891), the site of hematopoiesis as well as the relatedness between the different types of hemocytes remain thorny questions in studies of bivalves (Vogt, 2012; Kuchel et al., 2011). In the mollusk *Biomphalaria glabrata*, an amebocyte-producing organ (APO) has been described based upon the observation in phase contrast microscopy of mitoses in the cardiac region (Jeong et al., 1983). Moreover, infestation by parasites appeared to increase the mitotic index of APO (Salamat and Sullivan, 2008) while other investigations (dos Santos Souza and Araujo Andrade, 2012) underlined the need for specific markers to characterize precursors and differentiated hemocytes in order to settle this matter in *B. glabrata*.

Indeed, bivalves are not easily amenable to genetics, and while genomic data were published only recently (Zhang et al., 2012), these organisms are phylogenetically distant from main biological models. Meanwhile, farming of bivalves, a worldwide industry, notably with the Pacific oyster, *Crassostrea gigas* Thunberg 1793, is threatened by infectious diseases from viral, bacterial and protozoan etiology (Comps et al., 1976; Farley et al., 1972; Binesse et al., 2008; Cochennec-Laureau et al., 2003), which stresses the need for a better knowledge of hemocyte biology. The origin of hemocytes and, consequently, the location of the hematopoietic organ thus remain fundamental questions in bivalves, in particular with regard to the key role played by hemocytes in the cell-mediated immune defense (Duperthuy et al., 2011) and, moreover, the long-term production and physiology of the yet-to-be-described mollusk stem cells that are essential to the extreme longevity of certain bivalves (Butler et al., 2013).

Here we provide evidence for adult progenitor cells in bivalves and their differentiation into hemocytes in gill tissue. Analysis of the oyster (*C. gigas*) gill revealed irregularly folded structures (IFS) that displayed small round stem-like cells bathing into the hemolymph. Bromodeoxyuridine (BrdU) labeling revealed that the stem-like cells in the gill epithelium and in the nearby hemolymph actively replicated DNA. Proliferation of stem-like cells was further evidenced in gill by the detection of phosphorylated-histone H3, a mitosis marker (Minakhina et al., 2007). The existence of a population of stem and/or precursor cells in the oyster was established by the detection of Sox2, a marker for stemness (Liu et al., 2013), which is particularly abundant in the IFS epithelial cells. Hematopoiesis was evidenced by the co-expression of Sox2 and

[1]Universités Montpellier 2 et 1, Montpellier, 34095 France. [2]CRBM CNRS UMR 5237, Montpellier, 34293 France. [3]IGMM CNRS UMR 5535, Montpellier, 34293 France. [4]IGH CNRS UPR 1142, Montpellier, 34396, France. [5]Université de Strasbourg, Strasbourg, 67081 France. [6]IPHC CNRS UMR7178, Strasbourg, 67037 France. [7]IFREMER, LGP, La Tremblade, 17390 France.

*Author for correspondence (claude.delsert@crbm.cnrs.fr)

Received 15 April 2014; Accepted 10 June 2014

The Journal of Experimental Biology (2014) doi:10.1242/jeb.106575

List of abbreviations

BrdU	bromodeoxyuridine
ECM	extracellular matrix
FACS	fluorescence-activated cell sorting
FLN	Filamin
IFS	irregularly folded structure
IHC	immunohistochemistry
MS	mass spectrometry
MS/MS	tandem mass spectrometry
PBS	phosphate buffered saline
PMSF	phenyl methyl sulfonyl fluoride
SOD	superoxide dismutase
TOF	time-of-flight

Cu/Zn superoxide dismutase (SOD), a hemocyte-specific enzyme (Gonzalez et al., 2005) in gill cells. Finally, hematopoiesis was confirmed by the detection of Filamin (FLN), a protein specific for a sub-population of hemocytes (Rus et al., 2006), in large BrdU-labeled cells bathing in the hemolymph of gill vessels. We thus propose that the gill is the long-searched-for hematopoietic organ in bivalves (Cuénot, 1891).

RESULTS

Stem-like cells exist in the gill epithelium and hemolymph

The general structure of the oyster gill (reviewed in Galtsoff, 1964; Eble and Scro, 1996) is briefly recalled here for the purpose of this work, and further histological details are provided. The two oyster gills are both made of two V-shaped demi-branches each composed of an ascending and a descending lamella delimiting a water tube and linked by interlamellar junctions (supplementary material Fig. S1A,B). Each lamella is a succession of regularly folded structures, termed plicas, which are made of the repetition of a tubular structural unit called filament. The central part of the filament is occupied by a space filled with hemolymph while the basal part of the filament consists of a more or less regular layer of tightly packed and non-ciliated cells referred to as the epithelium (Galtsoff, 1964; Eble and Scro, 1996). Here, we examined in further detail the oyster gill organization.

Adult animals were collected during spring in the Mediterranean Sea. Scanning of hematoxylin & eosin stained cross-sections using a Nanozoomer revealed intriguing IFS in all examined samples (n=6; supplementary material Fig. S1C) in addition to the regularly folded structures described above. IFS were found to be made of a succession of stacks of eight or fewer long and thin parallel structures next to irregular folds, here referred to as tubules and convoluted structures, respectively (Fig. 1A; supplementary material Fig. S1B). The term epithelium is here conserved for the cell layer delimiting these structures because it defines the limit between the body and its environment, despite the fact that its organization does not correspond to a classical epithelial cell lining. Hematoxylin staining was intense in the epithelium and at the extremities of all tubules (Fig. 1A), which indicated a high concentration of nucleic acids. At higher magnification, nuclei appeared to be densely packed and surrounded by a thin and barely detectable eosin-stained

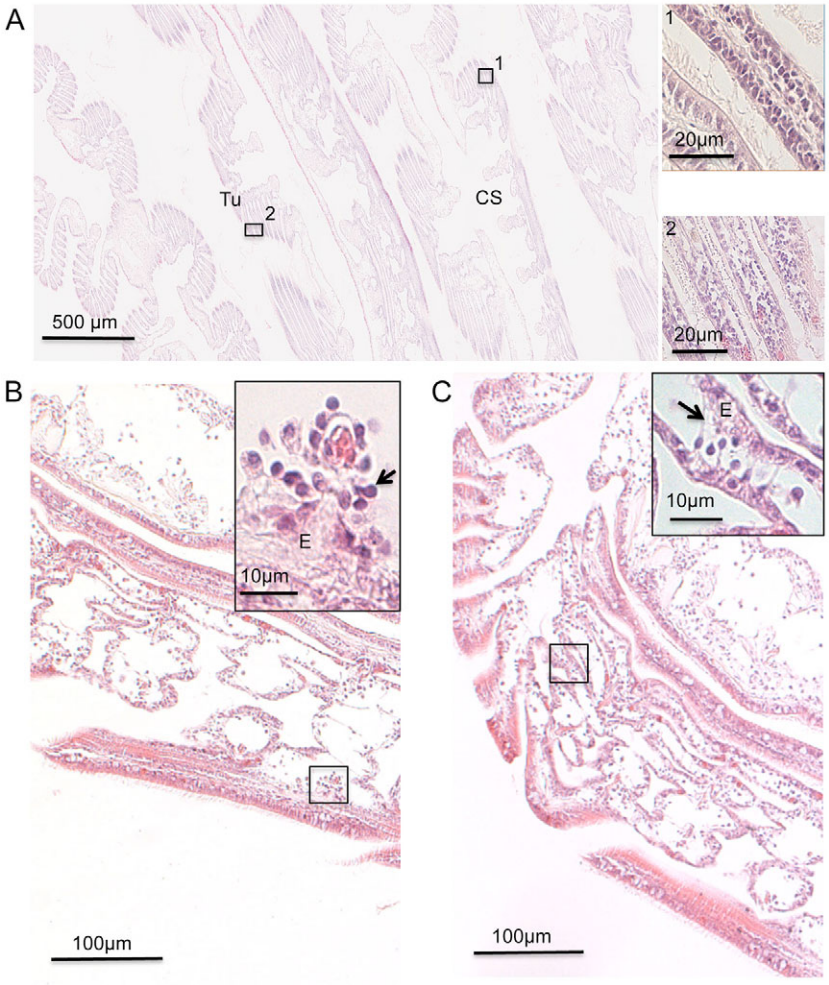

Fig. 1. Detail of an irregularly folded structure (IFS) region in the oyster *Crassostrea gigas*. (A) Scanning at low magnification shows the presence of stacks of tubules (Tu) and convoluted structures (CS). Higher magnification (1,2) revealed nuclei intensely stained with hematoxylin and surrounded with a thin and barely detectable eosin-stained cytoplasm. Note that nuclei are packed in the extracellular matrix (ECM) of the epithelium and at the extremities of the tubules. (B,C) Details of convoluted structures at higher magnification. (B) Small pear-shaped cells (inset, arrow) were seen burgeoning out of the ECM (E) into the hemolymph. (C) Long cytoplasmic extension of stem-like cells (inset, arrow) in the hemolymph of a tubule, in contact with the ECM.

The Journal of Experimental Biology

The Journal of Experimental Biology (2014) doi:10.1242/jeb.106575

cytoplasm (Fig. 1A, insets). The IFS epithelium is thus an irregular layer of cells, occurring in tight groups and embedded in a thick extracellular matrix (ECM) as shown in eosin-stained sections (Fig. 1A). The convoluted structures are less compact (Fig. 1B,C) and they are better suited to study the interaction between the epithelium and its environment. Taking advantage of the lesser density of the IFS, observation revealed small cells with a pear-shape nucleus, displaying no visible cytoplasm, which are morphological traits of stem cells (Rink, 2013). Some of these cells were barely attached to the tissue as if being released from the epithelial ECM into the hemolymph (Fig. 1B, inset, arrow). In addition, small cells with long and thin cytoplasmic extensions protruding inside the tubule's lumen (Fig. 1C, inset, arrow) were also observed in IFS. Interestingly, cytoplasmic protrusions are generally considered as an indication of cell movement (Lauffenburger and Horwitz, 1996).

Intense DNA replication occurs in the gill epithelium and hemolymph cells

One main characteristic of the hematopoietic tissue is to sustain a high level of DNA synthesis as exemplified by the *Drosophila* larval lymph gland (Jung et al., 2005).

To determine whether the gill is the site of intense DNA synthesis, entire gills (n=3) were cut out while preserving their superficial attachment region to the body. Cross-sections of the isolated gill (10 mm thick) were incubated for 16 h in L15 cell culture medium adjusted to seawater osmolarity and containing BrdU (25 µmol l^{-1}), a nucleotide analog, before immediate fixation. Paraffin cross-sections were submitted to immunohistochemistry (IHC) using a commercial mouse monoclonal anti-BrdU antibody. Fluorescence microscopy (Cy3) revealed a punctuated labeling typical of the DNA-incorporated BrdU in gill (Fig. 2). Labeling was particularly intense in the epithelium of the IFS tubules and convoluted structures (Fig. 2A1,2) but also in areas of the regular folds and the adjacent inter-lamellar junctions (Fig. 2A3–5), while no signal was detected in control sections (Fig. 2A6).

To determine whether DNA synthesis is more intense in gills than in other tissues, a solution of BrdU (1.6 mmol l^{-1}) was administered by injection to spats (n=3) for 6 h before fixation of the entire body of the animals. Fluorescence microscopy (Cy3) revealed BrdU labeling (supplementary material Fig. S2, BrdU) while autofluorescence was recorded in the green fluorescent protein channel (supplementary material Fig. S2, AF) to outline the tissues. The specificity of BrdU labeling was assessed by the absence of staining when primary antibody was omitted (supplementary material Fig. S2B,D,F). Examination at low magnification indeed showed that BrdU labeling was more intense in the IFS (supplementary material Fig. S2A) and in areas of the regularly folded gill (supplementary material Fig. S2C) than in the mantle (supplementary material Fig. S2E).

To further verify that BrdU incorporation corresponded to DNA synthesis and not to DNA reparation, the amount of cellular DNA was estimated using fluorescence-activated cell sorting (FACS) analysis, which allows the distinction between cells in G0 or G1 phase and cells replicating DNA (S phase) or sustaining mitosis (G2/M) (Vitale et al., 2013). FACS analysis (supplementary material Fig. S3A) of the cells dissociated from oyster (n=6) gills and mantles, following enzymatic incubation of minced tissues, revealed a higher percentage of S and G2/M phases in the gill (17.3%) than in the mantle (7.2%; supplementary material Fig. S3B,C). Moreover, cell counting revealed that cells dissociated from the gill were 6.3-fold more numerous than those dissociated from the mantle (supplementary material Table S1), which, together with the gill higher mitotic index (2.40-fold), indicates that the number of cells proliferating is much greater in the gill (15-fold) than in the mantle. These quantitative data are in agreement with the higher rate of BrdU incorporation observed in gill sections (Fig. 2A; supplementary material Fig. S2A,C), and indicate that BrdU incorporation indeed essentially corresponded to DNA synthesis.

Gill cross-sections, treated as above, were co-stained with fluorescent phalloidin, which binds F-actin and thus indicates the cytoplasm extent. Confocal microscopy revealed thin fluorescent rings around abundant BrdU-labeled nuclei in both the tubule epithelium and lumen (Fig. 3A), thus indicating that these stem-like cells undergoing replication in the IFS are almost devoid of cytoplasm. Observation at higher magnification (Fig. 3B, enlarged box of 3A) revealed small oblong stem-like cells massed in a tubule lumen (outlined by white lines). These cells appeared to be lined up in the direction of a less crowded part of the lumen (Fig. 3B, broken line). Interestingly, examination of a nearby sinus (Fig. 2B, outlined) revealed heterogeneity in the BrdU-labeled cells bathing in the hemolymph, of which sizes ranged from the small stem-like cells

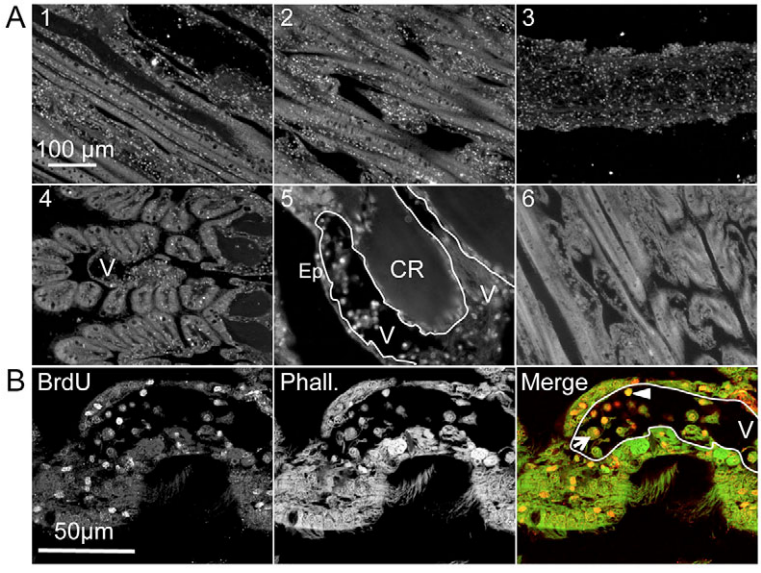

Fig. 2. Intense DNA replication in IFS of *C. gigas*. (A,B) Tissue was incubated for 16 h with bromodeoxyuridine (BrdU) in oyster cell culture before fixation and immunohistochemistry (IHC). (A) Fluorescent microscopy at low magnification revealed a widespread and intense BrdU labeling in IFS (1,2) and in a few areas of the regularly folded gill (3,4). (5) Higher magnification of a filament vessel (V, white outline) containing BrdU-labeled cells (scale bar, 25 µm). (6) No BrdU detection in control section. (B) Tissue section treated as above and with cytoplasm staining (green, Alexa 488-Phalloidin). Confocal image reveals that small stem-like cells (arrowhead) and large hemocyte-like cells (arrow) are labeled with BrdU in a gill vessel (V, white outline). CR, chitine rod; Phall., phalloidin.

The Journal of Experimental Biology (2014) doi:10.1242/jeb.106575

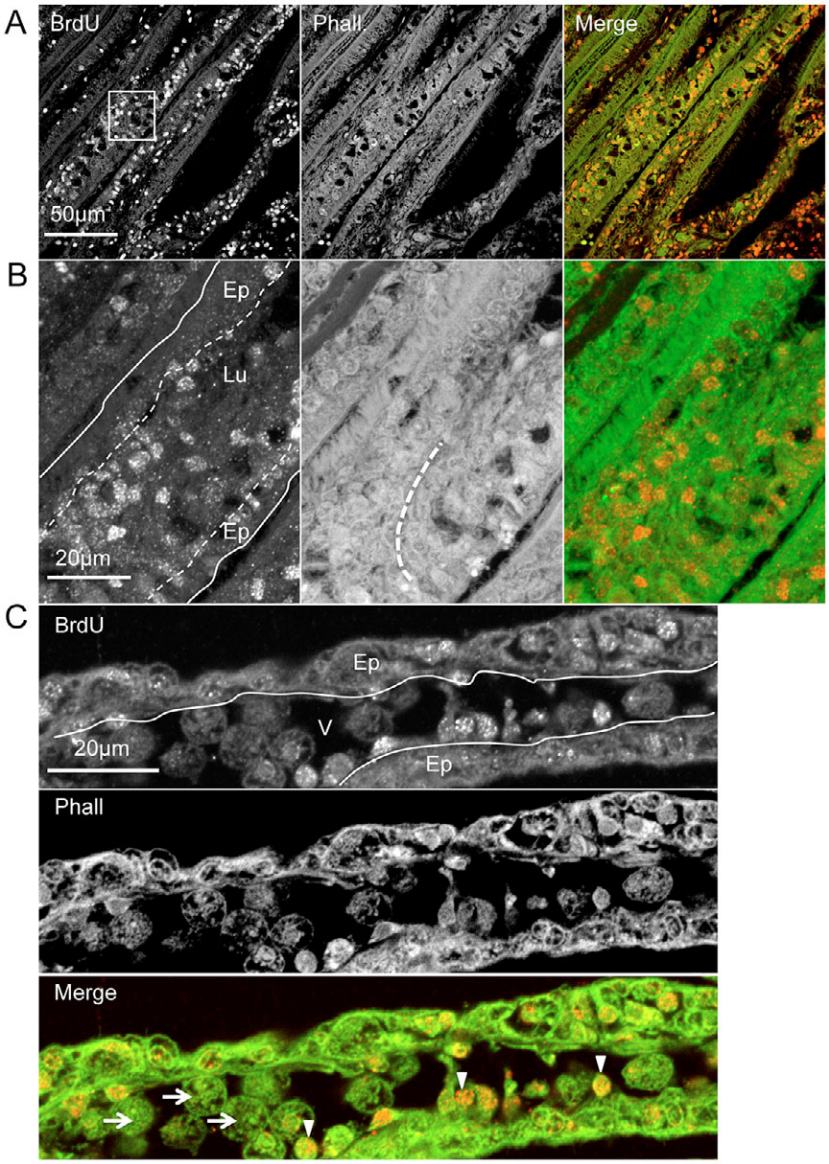

Fig. 3. DNA replication in stem-like cells inside a *C. gigas* tubule lumen. Images were acquired by confocal microscopy of tissue cross-sections after incubation with BrdU (25 µmol l^{-1}), fixation and IHC using BrdU mAb and Alexa 488-Phalloidin for cytoplasm visualization. (A) Observation after a 16 h BrdU-incubation revealed masses of cells dislaying BrdU labeling and a thin phalloidin-labeled cytoplasm inside the tubule lumen. (B) Observation at higher magnification (box in A) shows a mass of oblong stem-like cells in the tubule lumen (continuous and dashed lines delimit a tubule and its lumen, respectively), which are lined up (Phall., dashed line). (C) Observation of an IFS section showing a vessel (V, delimited by white lines) after a short (2 h) BrdU labeling. Note that the small cells with a thin cytoplasm are BrdU labeled (arrowheads) while the larger hemocyte-like cells are not (arrows). Ep, epithelia; Lu, lumen.

(arrowhead) to what could be large hemocytes (arrow). These data suggest that cells that incorporated BrdU may later differentiate into hemocytes because hemocytes do not replicate DNA (Hartenstein, 2006). To study this interesting possibility, gill cross-sections were labeled with BrdU for a short period of time (2 h) and immediately fixed and submitted to IHC as above. Under these conditions, a clearly detectable BrdU signal was again observed in the stem-like cells inside the lumen of a sinus (Fig. 3C, arrowheads). But in contrast, under these conditions no BrdU labeling was detected in the surrounding large hemocytes (Fig. 3C, arrows).

This result shows that, as expected, the large hemocytes did not incorporate BrdU during the 2 h incubation. Furthermore, it strongly suggests that the BrdU-positive stem-like cells could differentiate into hemocytes, explaining the existence of a BrdU-positive hemocyte population following a long BrdU incubation (Fig. 2B, arrow).

Cells proliferate in the gill epithelium and hemolymph

Cell proliferation is a distinctive feature of the lymph gland tissue in adult animals (Parslow et al., 2001). Cell proliferation was assayed using a commercial antibody against the phosphorylated (Ser10) histone H3 (H3PAb), a widely used mitosis marker, notably in *Drosophila* (Minakhina et al., 2007). Specificity of H3PAb for the oyster H3P was assayed on an immunoblot carrying gill chromatin extracts, which revealed a unique band corresponding to the expected molecular weight for the oyster histone H3 (15 kDa; EKC28030), while no band was observed on the corresponding non-chromatin supernatant (supplementary material Fig. S4A).

IHC was carried out on cross-sections of oysters (n=3) using H3PAb and DAPI to stain DNA. Confocal images revealed H3P-positive nuclei in both the mantle (Fig. 4A) and gill (Fig. 4B), although the H3P signal appeared much more abundant in the gill, while it was absent in the negative control (Fig. 4C). For quantification, contiguous confocal microscope fields were recorded at low magnification (×20) and counted for H3P and DAPI in both the mantle and gill (supplementary material Tables S2, S3).

The percentage of H3P-positive cells was quite high for gills (21.8%) when compared with mantles (4.7%, n=3; Fig. 4D). Moreover, measurement of the tissue surface in the corresponding microscope fields, using ImageJ software, provided density values of 0.192 and 0.005 H3P-positive nuclei per 100 µm^2 for the gill and mantle, respectively (Fig. 4E). Thus the gill higher cell density and mitotic index show that more cells divide in the gill than in the

The Journal of Experimental Biology (2014) doi:10.1242/jeb.106575

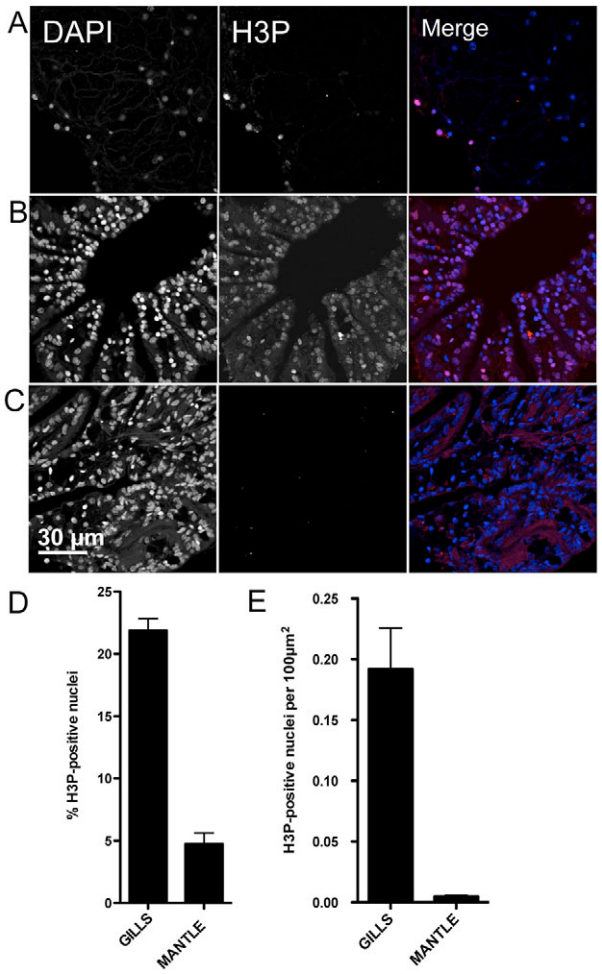

Fig. 4. Mitoses in the *C. gigas* gill and mantle tissues. Cross-sections were submitted to IHC using a rabbit anti-H3P antibody (red) and DAPI (blue) and were analyzed through confocal microscopy. (A) Image of a section of the mantle that reveals a few H3P-labeled cells (red) in this tissue, which is essentially made up of a few scattered large cells. (B) Image of a section of the regularly folded gill showing a high density of nuclei (DAPI) of which a fair proportion are H3P-positive (red). (C) Image of a control gill section treated as above while no anti-H3P antibody was used. (D,E) Quantification of the H3P-labeled cells in mantle and gill sections. Counting was carried out on at least 1000 nuclei on representative views for each animal (n=3). (D) Mitotic index in the oyster gill and mantle. The percentage of mitotic nuclei is 21.7 and 4.7% in the gill and mantle, respectively. (E) Density of mitotic nuclei per 100 µm^2. The density of mitotic nuclei is much higher in the gill (0.192±0.034 nuclei 100 µm^{-2}) than in the mantle (0.005±0.0009 nuclei 100 µm^{-2}).

mantle, which confirms the indirect evidence by FACS analysis (supplementary material Fig. S3).

Stem and/or precursor cells are abundant in the gill

Stem and precursor cells express specific markers such as the transcription factor Sox2 (Liu et al., 2013). A commercial anti-Sox2 antibody specifically revealed a unique band migrating according to the oyster Sox2 predicted molecular weight (36 kDa; EKC24855) on an immunoblot carrying oyster gill extract (supplementary material Fig. S4B). IHC was carried out on gill cross-sections using Sox2 antibody and DAPI. Confocal microscopy revealed a striking abundance of Sox2-positive nuclei in the gill (Fig. 5A), particularly, as shown at higher magnification, on cells clustered in the IFS epithelium (Fig. 5B). Moreover, Sox2 was found decorating loosely associated cells (Fig. 5C, stars) that filled the tubule's lumen (Fig. 5C, Lu), in a manner similar to that of the groups of stem-like cells observed through histology (insets in Fig. 1B,C) or BrdU labeling (Fig. 3B).

Altogether, our data show that the gill contains an abundance of stem and/or precursor Sox2-positive cells, some of which localized into the hemolymph.

Progenitor cells differentiate into hemocytes in the gill

IHC was performed on cross-sections using Sox2 antibody and a mouse antibody against the Zn/Cu SOD, an enzyme that is specifically expressed in oyster hemocytes (Duperthuy et al., 2011; Gonzalez et al., 2005). The epithelial cells of the IFS tubules (Fig. 6A, Tu) were intensely labeled for Sox2, as seen above, while fewer cells were labeled in the rest of the tissue (Fig. 6A; supplementary material Fig. S5). By contrast, and very strikingly, SOD-labeled cells were mostly restricted to the vessel adjacent to the tubules (Fig. 6A; supplementary material Fig. S5). We emphasize from these data that cells that are co-stained for Sox2 and SOD are likely to be progenitors (Sox2-positive) differentiating into hemocytes (SOD-positive). The fact that the co-stained cells are not localized in the tubule area (Tu) but mostly in the underlying connective tissue (Co) and vessels (V) (Fig. 6A; supplementary material Fig. S5) suggests that progenitors may migrate from the tubules towards the IFS vessel. This striking distribution of Sox2 and SOD markers is a general feature of the IFS structures as further shown at lower magnification in supplementary material Fig. S5.

To confirm that gill precursors differentiate into hemocytes, another hemocyte marker, FLN, was used. Indeed, this large actin-binding protein is specific for a subclass of hemocytes carrying out the encapsulation of parasites in *Drosophila* (Rus et al., 2006), the lamellocytes. Interestingly, encapsulation has also been described in mollusks (Loker and Bayne, 2001). The oyster FLN was purified to homogeneity (supplementary material Fig. S6A) and its identity was confirmed through mass spectrometry (supplementary material Table S4). A rabbit antibody was raised and immuno-purified (FLNAb) against the FPLC-purified oyster protein. Specificity of FLNAb was shown by an immunoblot using gill extract (supplementary material Fig. S4C) that revealed a protein migrating well over the 250 kDa marker, which is in agreement with the oyster FLN molecular weight (323 kDa; EKC28512.1).

IHC was performed on oyster cross-sections using FLNAb, SODAb and DAPI. Confocal microscopy confirmed FLNAb specificity because it revealed an intense and specific signal in the gonad axillary cells (supplementary material Fig. S6B) as previously shown for *Drosophila* (Sokol and Cooley, 2003). Furthermore, confocal microscopy revealed a sub-population of cells bathing into the IFS sinuses and vessels, which were confirmed to be hemocytes for their SOD co-labeling (supplementary material Fig. S6C).

Using this tool, we addressed whether gill precursors indeed differentiate into hemocytes. Thick cross-sections of gill tissue were incubated for 16 h with BrdU as above and immediately fixed. IHC was then carried out on gill cross-sections using first the FLNAb and then, after acidic denaturation, the anti-BrdU mAb. Fluorescence microscopy revealed strong signals for both FLN and BrdU in cells bathing in the hemolymph, notably of a main gill blood vessel (Fig. 6B,C).

This latter result is particularly significant as it shows that the stem and/or precursor cells replicated DNA and differentiated into hemocytes expressing the FLN marker in this isolated piece of the oyster gill.

The Journal of Experimental Biology (2014) doi:10.1242/jeb.106575

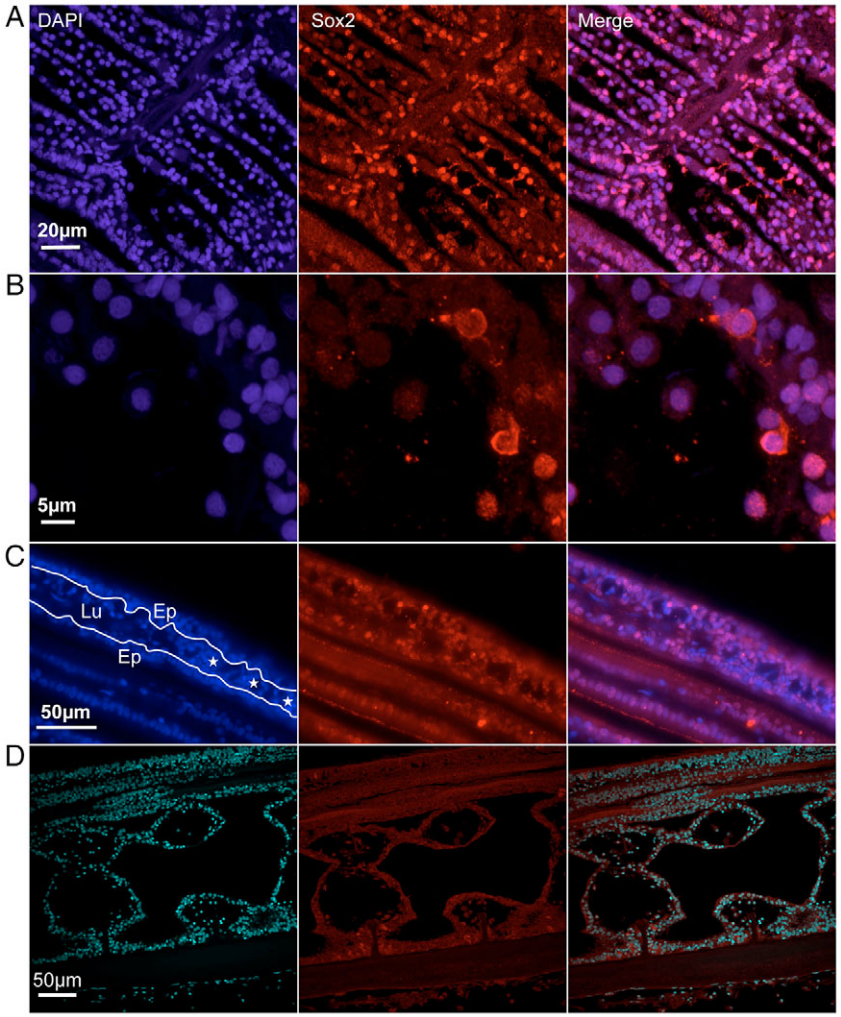

Fig. 5. Abundance of precursor cells in the IFS of *C. gigas*. Images acquired through fluorescence (C) or confocal microscopy (A,B,D) following IHC using a rabbit Sox2 antibody (red) and DAPI (blue). (A) Numerous IFS epithelial cells are Sox2-positive. Note that long cytoplasmic extensions as shown in Fig. 1C (inset) are occasionally decorated with Sox2. (B) At higher magnification, Sox2 decorates the nucleus of gill epithelial cells as well as the cytoplasm of a few small teardrop-shaped cells similar to the stem-like cells in Fig. 1B (inset). (C) Groups of Sox2-labeled cells (stars) loosely associated inside the hemolymph lumen (Lu, outlined in white) of an IFS tubule. Ep, epithelium. (D) Tissue section treated as above but without primary Sox2 antibody.

DISCUSSION

The aim of this research was to address the origin of hemocytes in bivalves. This question was complicated by the fact that the existence of adult somatic progenitor cells had not been shown.

In bivalves, immunity involves both cell-mediated and humoral systems. Although the effectors of the humoral defense, including soluble lectins, lysosomal enzymes (e.g. acid phosphatase, lysozyme) and anti-microbial peptides (Gueguen et al., 2006; Gueguen et al., 2009; Gonzalez et al., 2007a; Gonzalez et al., 2007b; Rosa et al., 2011), are synthesized by both hemocytes and epithelial cells (Itoh et al., 2010, Xue et al., 2010), the cell-mediated immune defense is exclusively performed by hemocytes (reviewed in Schmitt et al., 2012). Indeed, hemocytes are capable of non-self recognition, chemotaxis and active phagocytosis (Cheng, 1981). Moreover, hemocytes are implicated in cytotoxic reactions by the production of hydrolytic enzymes (Cheng and Rodrick, 1975), reactive oxygen species (Bayne, 1990; Pipe, 1992; Lambert et al., 2007; Aladaileh et al., 2007; Butt and Raftos, 2008; Boulanger et al., 2006; Kuchel et al., 2010), antimicrobial peptides and/or proteins (Gueguen et al., 2006; Gueguen et al., 2009; Gonzalez et al., 2007a; Gonzalez et al., 2007b; Rosa et al., 2011) and phenoloxidases, a class of copper proteins involved in melanization, an immune defense reaction associated with the encapsulation of larger parasites (Luna-Acosta et al., 2011). Beside their immunological functions, mollusk hemocytes are believed to be involved in shell mineralization (Mount, 2004), excretion, metabolite transport and digestion, and wound repair (reviewed in Cheng, 1996).

Yet, despite the multiple hemocyte functions that have been studied, the origin of hemocytes in bivalves has remained elusive since L. Cuénot (Cuénot, 1891) published his founding work on the origin of blood cells in animals. Even more striking is the fact that, although mollusks are models for a spectrum of research including frontier science in neurobiology (Landry et al., 2013) or ageing (Philipp and Abele, 2010), little is known about mollusk adult somatic stem cells. Recently, Vogt (Vogt, 2012), while reviewing invertebrate stem cells, revived the question of the existence and most importantly the long-term protection of stem cells in the extremely long-lived bivalves (Philipp and Abele, 2010).

Here we re-examined the origin of bivalve hemocytes by scrutinizing adult *C. gigas* tissues and identifying markers for both bivalve progenitor cells and hemocytes. While focusing on the gill for its overall higher density of nuclei as shown through histology and IHC, a less dense structure termed the IFS was uncovered, which contains a population of small stem-like cells (Fig. 1). Interestingly, although IFS occupies a variable proportion of the gill (one-sixth to one-fifth of a gill section), it was consistently highlighted in IHC when using markers for cell proliferation or for stemness, which emphasizes the IFS contribution to precursor cell proliferation in gills. In addition, histology suggested that a fraction of stem-like cells were only loosely attached to the IFS epithelium whereas in other places they produced long protrusions inside the

The Journal of Experimental Biology (2014) doi:10.1242/jeb.106575

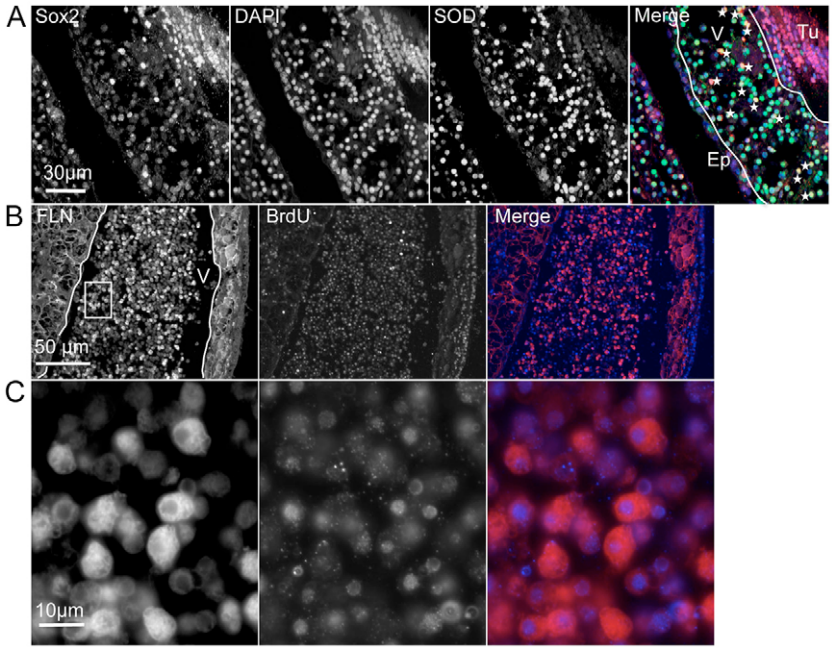

Fig. 6. Small cells displaying markers for stemness and for hemocytes in the IFS of *C. gigas*. (A) Hemocyte progenitors co-stained with Sox2 and SOD. IHC was carried out using a rabbit Sox2 antibody (red), a mouse superoxide dismutase (SOD) antibody specific for hemocytes (green), and DAPI (blue). The IFS, composed of several layers of Sox2-positive cells, is located in the tubule region (Tu), whereas SOD-positive cells, the hemocytes, are essentially located in a nearby vessel (V, white outline). Similarly, cells co-labeled for Sox2 and SOD (stars) are mostly located in the vessel, which suggests that progenitor cells may differentiate into hemocytes as they move towards the vessel (see also supplementary material Fig. S5). Ep, epithelium. (B) Precursor cells replicate DNA and differentiate into hemocytes in the gill. A 10-mm-thick cross-section of the gill was incubated with 25 µmol l^{-1} BrdU for 16 h before fixation and IHC. BrdU-labeled DNA (blue) and Filamin (FLN; red) were revealed as described above. Fluorescent microscopy revealed an abundance of large cells labeled for BrdU and FLN in the hemolymph of a main vessel at the base of the gill. (C) High magnification of B. FLN-stained cells harbor a typical punctuated nuclear BrdU labeling.

tubules. Interestingly, these cytoplasmic extensions are usually recognized as indicative of cell motion (Lauffenburger and Horwitz, 1996). Therefore, the stemness traits of these small cells in contact with the hemolymph raised the possibility that they participate in hematopoiesis in the oyster.

Hematopoiesis requires precursor cell proliferation as exemplified by the daily production of 10^{11} blood cells in human adults. The production of hemocytes can be deduced from the hemocyte population size and half-life. Indeed, the complete blood collection of an experimental oyster (10 g of meat) routinely provides 10^{6} hemocytes (Rolland et al., 2012), which is a conservative value because the proportion of blood cells infiltrating the oyster tissues is unknown. In contrast, the hemocyte half-life was determined to be 22 days for the related eastern oyster, *C. virginica* (Feng and Feng, 1974), a value consistent with the 28 days found for another bivalve, *Mercenaria mercenaria* (McIntosh and Robinson, 1999). Based upon these values, the lower range for the daily loss of hemocytes can be estimated at 22.000 h day^{-1} for a medium-sized individual. As a matter of fact, several lines of evidence corroborate this observation. First, the importance of apoptosis in the functioning of the mollusk immune system is reflected by the detection of high baseline apoptosis rates that range from 5 to 25% in circulating hemocytes and can reach to up to 50% in infiltrating tissue hemocytes (Sunila and LaBanca, 2003; Sokolova et al., 2004; Goedken et al., 2005; Cherkasov et al., 2007). This high rate of apoptosis is tied to the immune defense not only against parasites and pathogens, but also against toxic environments. Both *in vivo* and *in vitro* infections were shown to result in hemocyte phagocytosis, respiratory burst and finally in apoptosis (Goedken et al., 2005). In addition, detoxification of environmental pollutants, including of toxic substances produced by harmful algal blooms, has been shown to induce massive apoptotic death among the hemocyte population in bivalves (Medhioub et al., 2013; Ray et al., 2013; Yao et al., 2013; Prado-Alvarez et al., 2013). Finally, a physiological process not related to immune defense, shell mineralization, also leads to an important loss of hemocytes because it requires the migration of numerous hemocytes to the surface of the shell-facing outer mantle epithelium (Mount et al., 2004). A high capacity of hemocytes production is therefore expected in oysters and most likely in other bivalves.

DNA replication, here used as an indicator of cell division, was shown through BrdU labeling (Fig. 2; supplementary material Fig. S2) to be at a higher rate in the gill than in the mantle, another main tissue. Moreover, the percentage of cells with a DNA content indicative of cells engaged in division was also significantly higher in the gill than in the mantle, as shown by FACS analysis (supplementary material Fig. S3).

Cell proliferation was confirmed in the gill using the histone H3P, a mitotic marker. Indeed, counting the H3P-positive versus DAPI nuclei on confocal cross-sections confirmed that gill cells have quite a higher mitotic index than mantle. Furthermore, the higher cell density in the gill than in the mantle, a lacunar tissue (Galtsoff, 1964; Eble and Scro, 1996), translates into a much higher density of dividing cells in the gill (Fig. 4E). Gill therefore appears to have a superior capacity of generating cells.

In healthy adults, cell proliferation is likely to occur only in the hematopoietic organ in which blood cell progenitors are expected to be abundant. Indeed, the striking abundance of Sox2-positive cells in the gill, notably in the IFS epithelium and hemolymph (Fig. 5), confirmed our initial hypothesis that the small round cells with a pear-shaped nucleus seen through histology (Fig. 1) were stem or progenitor cells. Together, these data demonstrate the existence of adult somatic progenitor cells in mollusks, a prerequisite for hematopoiesis (Hartenstein, 2006).

Interestingly, cells that proliferate or express Sox2 in the IFS hemolymph mostly belong to groups of loosely associated cells (Fig. 3B, Fig. 5C), which is reminiscent of the electron microscopy description of the hematopoietic clusters of the polychaete annelid *Nicolea zostericola* (Hartenstein, 2006; Eckelbarger, 1976).

In addition, the IFS epithelium is embedded in a thick eosin-stained ECM from which stem-like cells emerge (Fig. 1). It is noteworthy that the epithelial ECM is a major component of the stem cell niche (reviewed in Watt and Huck, 2013). Indeed, it was recently shown that the alteration of the lymph gland ECM, as a result of the loss of the proteoglycan Perlecan/troll, reduces the

proliferation of progenitor cells in *Drosophila* (Dragojlovic-Munther et al., 2013; Grigorian et al., 2013).

Interestingly, SOD, a hemocyte-specific enzyme (Duperthuy et al., 2011; Gonzales et al., 2005), revealed an intriguing IFS spatial partition between the Sox2-positive stem and/or progenitor cells in the tubules and the hemocytes in the underlying vessels (Fig. 6A; supplementary material Fig. S5). Moreover, cells co-labeled for Sox2 and SOD are also mostly in the underlying connective tissue and vessels. This striking partitioning suggests that the Sox2-positive progenitor cells might differentiate into hemocytes while moving towards the gill vessels.

FLN, a large protein expressed in *Drosophila* lamellocytes, hemocytes that are involved in the defense against parasites (Rus et al., 2006; Sokol and Cooley, 2003), was shown to characterize a sub-population of oyster hemocytes (supplementary material Fig. S6C). Interestingly, the recent finding that FLN RNA is overexpressed in the hemocyte population of oysters infested with parasites (Morga et al., 2011) suggests that the FLN-positive hemocytes might indeed be lamellocytes.

The FLN marker was used to further show that an isolated piece of oyster gill constitutes a biological system in which progenitor cells can replicate DNA and differentiate into hemocytes (Fig. 6B,C), thus unambiguously showing that hematopoiesis occurs in the gill. Therefore, we believe that altogether our data show that the gill is a significant contributor to hematopoiesis in the oyster *C. gigas*.

While the evidence for adult somatic stem cells provided by this work should have an impact on mollusk biology as it did in other biological systems, a direct implication of these findings is expected on studies including: (1) the maintenance of stem cells in extremely long-lived bivalves, (2) the life-long growth of tissues in bivalves and graft in pearl oysters, (3) the mollusk neoplasia notably in farmed bivalves and (4) the development of mollusk continuous cell culture.

MATERIALS AND METHODS

Animals and hemolymph collection

Adult *C. gigas* (15–20 g of meat) and spat (1.8 g of meat) were purchased from local oyster farms in Palavas-les-Flôts (Gulf of Lion, France).

Reagents

All chemicals were from Sigma-Aldrich (St Louis, MO, USA) unless otherwise mentioned.

Histochemistry and IHC

Tissues were fixed using Davidson's fixative (for 1 liter: 330 ml 95% ethyl alcohol, 220 ml 37% formaldehyde solution, 115 ml glacial acetic acid, 335 ml filtered seawater) at 4°C for 16 h. Tissue samples were then dehydrated in 70, 80 and 96% successive ethanol baths and then twice in Xylene before embedding in paraffin. Cross-sections (5 µm thick) were cut using an HM355S microtome (Thermo Scientific, Illkirch, France) and then dried O/N at 37°C. Paraffin was eliminated in Xylene bathes and sections were then rehydrated in successive 96% to 70% ethanol baths and then in TBST [50 mmol l^{-1} Tris (8.0), 150 mmol l^{-1} NaCl, 0.05% Tween 20].

For histology, tissue slides were incubated with hematoxylin for 2 min and then counterstained for 4 min with eosin G (0.5% ethanol), and washed in 100% ethanol and xylene before mounting in Mountex medium (Histolab, Seoul, Korea).

For IHC, sections were permeabilized for 1 h in 0.2% Triton in TBST solution containing 5% fat-free milk. Sections were incubated with primary antibodies diluted in 2% bovine serum albumin in TBST overnight in a humid chamber at 4°C.

During co-detection of protein and BrdU, BrdU was detected in a second step. After protein revelation with fluorescent secondary antibody, a 2 mol l^{-1} HCl denaturation step was carried out for 30 min at 37°C before instant renaturation using 0.1 mol l^{-1} Borax (pH 9.0) and several rinses in TBST, before O/N incubation at room temperature with anti-BrdU monoclonal antibody.

Antibodies and immunopurification

Antibody characteristics and dilution

The following antibodies were used as described here: monoclonal anti-BrdU (B-8434, IgG1; Sigma-Aldrich) at a dilution of 1/500; rabbit polyclonal anti-H3P (06-570, immuno-purified; Merck Millipore, Darmstadt, Germany) at a dilution of 1/1000; rabbit polyclonal anti-Sox2 (ab97959, immuno-purified; Abcam, Cambridge, MA, USA) at a dilution of 1/1000; in-house mouse monoclonal anti-SOD (immuno-purified) at a dilution of 1/1000 (Gonzalez et al., 2005); an immunopurified in-house rabbit polyclonal anti-FLN antibody at a dilution of 1/1000.

Immunopurification

For immunopurification, purified FLN was covalently bound to CNBr-activated Sepharose™ 4 Fast Flow according to the manufacturer's recommendations (Sigma-Aldrich, Q1126). Immunopurification was performed as described previously (Cau et al., 2001). Immunopurified FLN antibody was used at a dilution of 1/1000. All of the secondary antibodies were prepared from affinity-purified goat antibodies that react with IgG heavy chains and all classes of immunoglobulin light chains from rabbit or mouse (Molecular Probes, Eugene, OR, USA): goat anti-rabbit Alexa 555 (A21429) at a dilution of 1/1000 and goat anti-mouse Alexa 488 (A11029) at a dilution of 1/1000. To reveal the rabbit anti-H3P, a biotinylated goat anti-rabbit (S323555) was used at a dilution of 1/500 and revealed using Avidin Alexa 647 (S21374, Molecular Probes) at a dilution of 1/1000. Secondary antibodies were incubated at room temperature for 1 h. When necessary, DAPI (Sigma-Aldrich, D8417) was added at a dilution of 1/3000 to the secondary antibody. Mounting medium for fluorescence microscopy was made as follows: 10 g of Mowiol (Sigma-Aldrich, 81381) and 2.5 g of DABCO (Sigma-Aldrich, 290734) were dissolved in 90 ml phosphate buffered saline (PBS; pH 7.4) and 40 ml glycerol was added. Aliquots of 500 µl were frozen at −20°C until use.

BrdU incorporation

A volume of 100 µl of a 1.6 mmol l^{-1} BrdU solution was injected in the sinus of the adductor muscle of oysters (1.8 g of meat, n=3), which were maintained in seawater at room temperature for 6 h before fixation of the entire body. Alternatively, thick body cross-sections were incubated as follows: one transversal section was carried out on the hedge of the heart chamber while the other parallel section was 10 mm away in the direction of the mouth (Galtsoff, 1964). Tissue sections were incubated in 50 ml of L15 cell culture medium (LifeSciences Invitrogen, Grand Island, NY, USA) adjusted to 1100 mOsm with sea salts and supplemented with 25 µmol l^{-1} ml^{-1} BrdU (B5002, Sigma-Aldrich) under mild stirring at 15°C for various lengths of time. Note that the BrdU concentration is low compared with the conditions used for mouse *in vivo* labeling (160 µmol l^{-1} kg^{-1} of tissue) (Magavi et al., 2008).

FACS analysis

The entire mantle and gills were harvested from oysters (15–20 g of meat, n=6). Tissues were minced and incubated with Pronase (20 µg ml^{-1}) in 1100 mOsm Hank's buffer containing no Ca^{2+} or Mg^{2+} with a gentle shaking overnight at 4°C. Supernatant was filtered (50 µm mesh) and debris was eliminated by several washes and centrifugations at low speed (100 ***g***) in Hank's buffer at 4°C for 10 min. Cells were then fixed on Davidson's fixative for 20 min at room temperature and washed in PBS after centrifugation at 100 ***g*** for 10 min. Pellets were resuspended in propidium iodide (50 µg ml^{-1}) in 0.1% (w/v) D-glucose in PBS supplemented with 1 µg ml^{-1} (w/v) RNase A and incubated for 30 min at 37°C and then overnight at 4°C. FACS acquisitions were performed using a FACSCalibur (BD Biosciences, San Diego, CA, USA) equipped with a 70 µm nozzle, and data were statistically evaluated using CellQuest™ (Becton Dickinson, Pont de Claix, France). Only the events characterized by normal forward scatter

and side scatter parameters were gated for inclusion in the statistical analysis (Vitale et al., 2013).

Chromatin extraction

Tissues were frozen in liquid nitrogen, pulverized in a press and homogenized using a tissue homogenizer in modified RIPA buffer (25 mmol l^{-1} Tris HCl, pH 7.4; 150 mmol l^{-1} NaCl; 5 mmol l^{-1} EDTA, 1% Triton, 10% glycerol, 50 mmol l^{-1} NaF and 10 mmol l^{-1} Na glycerophosphate) to which the following were added before use: 2 mmol l^{-1} dithiothreitol, 1 mmol l^{-1} Na_3VO_4, protease inhibitor cocktail, 1 mmol l^{-1} phenyl methyl sulfonyl fluoride (PMSF) and 1 mmol l^{-1} benzamidine (both diluted from fresh stock in isopropanol). All steps were carried out at 0°C. The extract was clarified at low speed for 5 min and the resulting supernatant was centrifuged at 10,000 ***g*** for 30 min in an SS34 rotor (ThermoFisher Scientific, Waltham, MA, USA). Aliquots of the supernatant were frozen at −80°C for control. The pellet was submitted to sonication (Branson 450D, Danbury, CT, USA) until resuspension. The extract was then submitted to several rounds of French press in order to further homogenize the oyster chromatin. Protein concentration of the chromatin extract was determined using the Bradford assay. Chromatin fractions were frozen at −80°C until further use. Chromatin samples were incubated in Laemmli buffer containing 50 mmol l^{-1} iodoacetate and again submitted to sonication before heating at 94°C for 10 min. Sample was loaded on a 12% SDS-PAGE and transferred to PVDF membrane (MerckMillipore, Darmstadt, Germany).

Purification of the oyster FLN

Oyster tissues were frozen in liquid nitrogen and ground to powder in a press. We were particularly careful to prevent protein degradation because this large protein (323 kDa) is labile. Typically, 30 g of powder was homogenized using a Polytron in 50 ml of 300 mmol l^{-1} KCl in buffer A [20 mmol l^{-1} Hepes/KOH (pH 7.5), 1 mmol l^{-1} $MgCl_2$, 0.1 mmol l^{-1} EDTA, 10% (v/v) glycerol, 1 mmol l^{-1} dithiothreitol 0.5 mmol l^{-1} PMSF and 1× protease inhibitor cocktail]. The extract was clarified by low-speed centrifugation into 50 ml Falcon tubes to pellet remaining tissue fragments. The supernatant was then submitted to 100,000 ***g*** ultracentrifugation on an SW28 rotor (Beckman Coulter, Villepinte, France) at 4°C for 1 h. The typical concentration for the S100 extract was 10 mg ml^{-1}. All chromatography resins were from GE Healthcare (Fairfield, CT, USA). Briefly, 2 ml of an S100 oyster protein extract was incubated in a 20 ml batch of SP Sepharose FF cation exchanger, rinsed with 35 mmol l^{-1} KCl in buffer A and eluted with 6 ml of 250 mmol l^{-1} KCl in buffer A. Supernatant was diluted to 35 mmol l^{-1} KCl in buffer A before injection in Q Sepharose HPLC. After rinsing with 35 mmol l^{-1} KCl in buffer A, elution was carried out with a linear gradient from 35 to 400 mmol l^{-1} KCl in buffer A. The elution peak, detected through absorbance at 280 nm, corresponded to the 250 mmol l^{-1} KCl fractions. Analysis of the protein elution peak was performed on Coomassie-stained 8% SDS-PAGE. Fractions containing an intense and high molecular weight band over the 250 kDa marker were pooled and diluted to 35 mmol l^{-1} KCl in buffer A before injection on an SP Sepharose FF cation exchanger, and further rinsed with 35 mmol l^{-1} KCl in buffer A and eluted with a linear gradient from 35 to 400 mmol l^{-1} KCl in buffer A. Fractions of the main peak eluted at 250 mmol l^{-1} KCl were pooled and analyzed as above. Positive elution fractions were diluted at 35 mmol l^{-1} KCl in buffer A before injection on a heparin Affigel column and rinsed with 35 mmol l^{-1} KCl in buffer A. Elution fractions (corresponded to 200 mmol l^{-1} KCl) were confirmed to contain the high molecular band as above (Fig. 6A). Positive fractions were precipitated with 70% ammonium sulfate at 4°C. Pellets were solubilized in electrophoresis buffer and denatured in Laemmli buffer without β-mercapto ethanol before electrophoresis on a 7% preparative SDS-PAGE. A unique band over 250 kDa was revealed using Colloidal Blue. The band was cut off the gel and it was analyzed through mass spectrometry (supplementary material Table S4), which provided an unambiguous signature for FLN.

FLN analysis

The mass spectrometry (MS) and tandem mass spectrometry (MS/MS) analyses were performed on the SYNAPT™, a hybrid quadrupole orthogonal acceleration time-of-flight (TOF) tandem mass spectrometer (Waters, Milford, MA, USA) equipped with a Z-spray ion source and a lock mass system. The capillary voltage was set at 3.5 kV and the cone voltage at 35 V. Mass calibration of the TOF was achieved using phosphoric acid (H_3PO_4) on the [50; 2000] *m*/*z* range in positive mode. Online correction of this calibration was performed with Glu-fibrino-peptide B as the lock-mass. The ion (M+2H) 2+ at *m*/*z* 785.8426 was used to calibrate MS data and the fragment ion (M+H)+ at *m*/*z* 684.3469 was used to calibrate MS/MS data during the analysis.

For MS/MS experiments, the system was operated with automatic switching between MS and MS/MS modes (MS 0.5 s $scan^{-1}$ on *m*/*z* range [250; 1500] and MS/MS 0.7 s $scan^{-1}$ on *m*/*z* range [50; 2000]). The three most abundant peptides (intensity threshold 60 counts s^{-1}), preferably doubly and triply charged ions, were selected on each MS spectrum for further isolation and CID fragmentation with two energies set using the collision energy profile. Fragmentation was performed using argon as the collision gas. The complete system was fully controlled by MassLynx 4.1 (SCN 566, Waters). Raw data collected during nanoLC-MS/MS analyses were processed and converted with ProteinLynx Browser 2.3 (Waters) into .pkl peak list format. Normal background subtraction type was used for both MS and MS/MS with a 5% threshold and a fifth-order polynomial correction, and deisotoping was performed.

Image quantification

Manual counting of H3P-positive cells (red) and DAPI (blue) was performed using the analyze/cell counter plugin of ImageJ software on several confocal images acquired using the ×20 objective. Total H3P-positive cells and total nuclei were summed for each animal. At least 1000 cells were counted for both gill and mantle for each animal (*n*=3). Error bars are s.e.m.

Microscopy

IHC images were viewed using a Zeiss Axioimager Z2 (Oberkochen, Germany) with a Zeiss 20X Plan Apo 0.8 and Zeiss 40X Plan Apo 1.3 Oil DIC (UV) VIS-IR. Micrographs were collected using a Coolsnap HQ2 CCD camera (Roper Scientific, Evry, France) driven by Metamorph 7.1 software (Molecular Devices). Confocal microscopy was performed using a Zeiss LSM780 Confocal with a Zeiss 40X PLAN APO 1.3 oil DIC (UV) VIS-IR. Series of optical sections were collected. Histology was viewed using a Nanozoomer (Hamamatsu, Massy, France) to provide both an overview and a detailed structure of gill. Images were analyzed using NDP view software (Hamamatsu).

Acknowledgements

We are indebted to M. Sassine for technical support and to A. Lengronne, B. Romestand and B. Pain for kindly providing antibodies. The authors thank T. Renault (LGP/Ifremer) and A. Abrieu (CRBM/CNRS) for support during the course of this work, the members of the CRBM, in particular D. Fesquet, M. Bellis and J.-C. Labbé for comments, and the Montpellier RIO Imaging facility for technical support.

Competing interests

The authors declare no competing financial interests.

Author contributions

M.J., N.M., P.C., J.C., J.-M.S. and C.D. performed experiments and analyzed data. C.D. designed the experiments and wrote the manuscript.

Funding

M.J. was supported by a grant of La Ligue Contre le Cancer. This work was supported by the ANR (http://www.agence-nationale-recherche.fr) grants 08-GENO-028-02 to N.M. and 10-INSB-08-03 to J.-M.S.

Supplementary material

Supplementary material available online at
http://jeb.biologists.org/lookup/suppl/doi:10.1242/jeb.106575/-/DC1

References

Aladaileh, S., Nair, S. V., Birch, D. and Raftos, D. A. (2007). Sydney rock oyster (*Saccostrea glomerata*) hemocytes: morphology and function. *J. Invertebr. Pathol.* **96**, 48-63.

Bayne, B. L. (1990). Phagocytosis and non-self recognition in invertebrates. *BioScience* **40**, 723-731.
Binesse, J., Delsert, C., Saulnier, D., Champomier-Vergès, M. C., Zagorec, M., Munier-Lehmann, H., Mazel, D. and Le Roux, F. (2008). Metalloprotease vsm is the major determinant of toxicity for extracellular products of *Vibrio splendidus*. *Appl. Environ. Microbiol.* **74**, 7108-7117.
Bodnar, A. G. (2009). Marine invertebrates as models for aging research. *Exp. Gerontol.* **44**, 477-484.
Boulanger, N., Bulet, P. and Lowenberger, C. (2006). Antimicrobial peptides in the interactions between insects and flagellate parasites. *Trends Parasitol.* **22**, 262-268.
Bureau, D., Hajas, W., Surry, N. W., Hand, C. M., Dovey, G. and Campbell, A. (2002). Age, size structure and growth parameters of geoducks (*Panopea abrupta*, Conrad 1849) from 34 locations in British Columbia sampled between 1993 and 2000. *Can. Tech. Rep. Fish. Aquat. Sci.* **2413**, 1-84.
Butler, P. G., Wanamaker, A. D., Scourse, J. D., Richardson, C. A. and Reynolds, D. J. (2013). Variability of marine climate on the North Icelandic Shelf in a 1357-year proxy archive based on growth increments in the bivalve *Arctica islandica*. *Palaeogeogr. Palaeoclimatol. Palaeoecol.* **373**, 141-151.
Butt, D. and Raftos, D. (2008). Phenoloxidase-associated cellular defence in the Sydney rock oyster, *Saccostrea glomerata*, provides resistance against QX disease infections. *Dev. Comp. Immunol.* **32**, 299-306.
Cau, J., Faure, S., Comps, M., Delsert, C. and Morin, N. (2001). A novel p21-activated kinase binds the actin and microtubule networks and induces microtubule stabilization. *J. Cell Biol.* **155**, 1029-1042.
Cheng, T. C. (1981). Invertebrates blood cells. In *Bivalves* (ed. A. N. Ratcliffe and F. A. Rowley), pp. 233-301. London: Academic Press.
Cheng, T. (1996). Hemocytes: forms and functions. In *The Eastern Oyster Crassostrea virginica* (ed. V. S. Kennedy, R. I. E. Newell and A. F. Eble), pp. 299-326. Trenton, MD: University of Maryland Medical System.
Cheng, T. C. and Rodrick, G. E. (1975). Lysosomal and other enzymes in the hemolymph of *Crassostrea virginica* and *Mercenaria mercenaria*. *Comp. Biochem. Physiol.* **52B**, 443-447.
Cherkasov, A. S., Grewal, S. and Sokolova, I. M. (2007). Combined effects of temperature and cadmium exposure on haemocyte apoptosis and cadmium accumulation in the eastern oyster *Crassostrea virginica* (Gmelin). *J. Therm. Biol.* **32**, 162-170.
Cochennec-Laureau, N., Auffret, M., Renault, T. and Langlade, A. (2003). Changes in circulating and tissue-infiltrating hemocyte parameters of European flat oysters, Ostrea edulis, naturally infected with *Bonamia ostreae*. *J. Invertebr. Pathol.* **83**, 23-30.
Comps, M., Bonami, J. R., Vago, C. and Campillo, A. (1976). Une virose de l'huître portugaise (*Crassostrea angulata* Lmk). *C. R. Acad. Sci. Paris* **282**, 991-993.
Cuénot, L. (1891). Le sang et les glandes lymphatiques. In *Archives de Zoologie Expérimentale et Générale* (ed. H. Lacaze-Duthiers), pp. 13-90. Paris: Académie des Sciences.
dos Santos Souza, S. and Araújo Andrade, Z. (2012). The significance of the amoebocyte-producing organ in *Biomphalaria glabrata*. *Memórias do Instituto Oswaldo Cruz* **107**, 598-603.
Dragojlovic-Munther, M. and Martinez-Agosto, J. A. (2013). Extracellular matrix-modulated Heartless signaling in *Drosophila* blood progenitors regulates their differentiation via a Ras/ETS/FOG pathway and target of rapamycin function. *Dev. Biol.* **384**, 313-330.
Duperthuy, M., Schmitt, P., Garzón, E., Caro, A., Rosa, R. D., Le Roux, F., Lautrédou-Audouy, N., Got, P., Romestand, B., de Lorgeril, J. et al. (2011). Use of OmpU porins for attachment and invasion of *Crassostrea gigas* immune cells by the oyster pathogen Vibrio splendidus. *Proc. Natl. Acad. Sci. USA* **108**, 2993-2998.
Eble, A. F. and Scro, R. (1996). General anatomy. In *The Eastern Oyster Crassostrea virginica* (ed. V. S. Kennedy, R. I. E. Newell and A. F. Eble), pp. 19-71. Trenton, MD: University of Maryland Medical System.
Eckelbarger, K. J. (1976). Origin and development of the amoebocytes of *Nicolea zostericola* (Polychaeta; Terebellidae) with a discussion of their possible role in oogenesis. *Mar. Biol.* **36**, 169-182.
Farley, C. A., Banfield, W. G., Kasnic, G., Jr and Foster, W. S. (1972). Oyster herpes-type virus. *Science* **178**, 759-760.
Feng, S. Y. and Feng, J. S. (1974). The effect of temperature on cellular reactions of *Crassostrea virginica* to the injection of avian erythrocytes. *J. Invertebr. Pathol.* **23**, 22-37.
Finch, C. E. and Austad, S. N. (2001). History and prospects: symposium on organisms with slow aging. *Exp. Gerontol.* **36**, 593-597.
Galtsoff, P. S. (1964). The gills. In *The American Oyster* (ed. S. L. Udall), pp. 121-151.. Washington, DC: US Department of the Interior.
Goedken, M., Morsey, B., Sunila, I., Dungan, C. and De Guise, S. (2005). The effects of temperature and salinity on apoptosis of *Crassostrea virginica* hemocytes and *Perkinsus marinus*. *J. Shellfish Res.* **24**, 177-183.
Gonzalez, M., Romestand, B., Fievet, J., Huvet, A., Lebart, M. C., Gueguen, Y. and Bachère, E. (2005). Evidence in oyster of a plasma extracellular superoxide dismutase which binds LPS. *Biochem. Biophys. Res. Commun.* **338**, 1089-1097.
Gonzalez, M., Gueguen, Y., Desserre, G., de Lorgeril, J., Romestand, B. and Bachère, E. (2007a). Molecular characterization of two isoforms of defensin from hemocytes of the oyster *Crassostrea gigas*. *Dev. Comp. Immunol.* **31**, 332-339.
Gonzalez, M., Gueguen, Y., Destoumieux-Garzón, D., Romestand, B., Fievet, J., Pugnière, M., Roquet, F., Escoubas, J. M., Vandenbulcke, F., Levy, O. et al. (2007b). Evidence of a bactericidal permeability increasing protein in an invertebrate, the *Crassostrea gigas* Cg-BPI. *Proc. Natl. Acad. Sci. USA* **104**, 17759-17764.
Grigorian, M., Liu, T., Banerjee, U. and Hartenstein, V. (2013). The proteoglycan Trol controls the architecture of the extracellular matrix and balances proliferation and differentiation of blood progenitors in the *Drosophila* lymph gland. *Dev. Biol.* **384**, 301-312.
Gueguen, Y., Herpin, A., Aumelas, A., Garnier, J., Fievet, J., Escoubas, J. M., Bulet, P., Gonzalez, M., Lelong, C., Favrel, P. et al. (2006). Characterization of a defensin from the oyster *Crassostrea gigas*. Recombinant production, folding, solution structure, antimicrobial activities, and gene expression. *J. Biol. Chem.* **281**, 313-323.
Gueguen, Y., Bernard, R., Julie, F., Paulina, S., Delphine, D. G., Franck, V., Philippe, B. and Evelyne, B. (2009). Oyster hemocytes express a proline-rich peptide displaying synergistic antimicrobial activity with a defensin. *Mol. Immunol.* **46**, 516-522.
Hartenstein, V. (2006). Blood cells and blood cell development in the animal kingdom. *Annu. Rev. Cell Dev. Biol.* **22**, 677-712.
Itoh, N., Okada, Y., Takahashi, K. G. and Osada, M. (2010). Presence and characterization of multiple mantle lysozymes in the Pacific oyster, *Crassostrea gigas*. *Fish Shellfish Immunol.* **29**, 126-135.
Jeong, K. H., Lie, K. J. and Heyneman, D. (1983). The ultrastructure of the amebocyte-producing organ in *Biomphalaria glabrata*. *Dev. Comp. Immunol.* **7**, 217-228.
Jung, S. H., Evans, C. J., Uemura, C. and Banerjee, U. (2005). The *Drosophila* lymph gland as a developmental model of hematopoiesis. *Development* **132**, 2521-2533.
Kuchel, R. P., Raftos, D. A., Birch, D. and Vella, N. (2010). Haemocyte morphology and function in the Akoya pearl oyster, *Pinctada imbricata*. *J. Invertebr. Pathol.* **105**, 36-48.
Lambert, C., Soudant, P., Jegaden, M., Delaporte, M., Labreuche, Y., Moal, J., Boudry, P., Jean, F., Huvet, A. and Samain, J. (2007). *In vitro* modulation of reactive oxygen and nitrogen intermediate (ROI/RNI) production in *Crassostrea gigas* hemocytes. *Aquaculture* **270**, 413-421.
Landry, C. D., Kandel, E. R. and Rajasethupathy, P. (2013). New mechanisms in memory storage: piRNAs and epigenetics. *Trends Neurosci.* **36**, 535-542.
Lauffenburger, D. A. and Horwitz, A. F. (1996). Cell migration: a physically integrated molecular process. *Cell* **84**, 359-369.
Liu, K., Lin, B., Zhao, M., Yang, X., Chen, M., Gao, A., Liu, F., Que, J. and Lan, X. (2013). The multiple roles for Sox2 in stem cell maintenance and tumorigenesis. *Cell. Signal.* **25**, 1264-1271.
Loker, E. S. and Bayne, C. J. (2001). Molecular studies of the molluscan response to digenean infection. *Adv. Exp. Med. Biol.* **484**, 209-222.
Luna-Acosta, A., Thomas-Guyon, H., Amari, M., Rosenfeld, E., Bustamante, P. and Fruitier-Arnaudin, I. (2011). Differential tissue distribution and specificity of phenoloxidases from the Pacific oyster *Crassostrea gigas*. *Comp. Biochem. Physiol.* **159B**, 220-226.
Magavi, S. S. and Macklis, J. D. (2008). Immunocytochemical analysis of neuronal differentiation. *Methods Mol. Biol.* **438**, 345-352.
McIntosh, L. M. and Robinson, W. E. (1999). Cadmium turnover in the hemocytes of *Mercenaria mercenaria* (L.) in relation to hemocyte turnover. *Comp. Biochem. Physiol.* **123C**, 61-66.
Medhioub, W., Ramondenc, S., Vanhove, A. S., Vergnes, A., Masseret, E., Savar, V., Amzil, Z., Laabir, M. and Rolland, J. L. (2013). Exposure to the neurotoxic dinoflagellate, *Alexandrium catenella*, induces apoptosis of the hemocytes of the oyster, *Crassostrea gigas*. *Mar. Drugs* **11**, 4799-4814.
Minakhina, S., Druzhinina, M. and Steward, R. (2007). Zfrp8, the Drosophila ortholog of PDCD2, functions in lymph gland development and controls cell proliferation. *Development* **134**, 2387-2396.
Morga, B., Arzul, I., Faury, N., Segarra, A., Chollet, B. and Renault, T. (2011). Molecular responses of *Ostrea edulis* haemocytes to an in vitro infection with Bonamia ostreae. *Dev. Comp. Immunol.* **35**, 323-333.
Mount, A. S., Wheeler, A. P., Paradkar, R. P. and Snider, D. (2004). Hemocyte-mediated shell mineralization in the eastern oyster. *Science* **304**, 297-300.
Parslow, T. G., Stites, D. P., Terr, A. I. and Imboden, J. B. (2001). *Medical Immunology*, 10th edn. Los Altos, CA: Lange Medical Publishers.
Peck, L. S. and Bullough, L. W. (1993). Growth and population structure in the infaunal bivalve *Yoldia eightsi* in relation to iceberg activity at Signy island, Antarctica. *Mar. Biol.* **117**, 235-241.
Philipp, E. E. and Abele, D. (2010). Masters of longevity: lessons from long-lived bivalves – a mini-review. *Gerontology* **56**, 55-65.
Pipe, R. K. (1992). Generation of reactive oxygen metabolites by the haemocytes of the mussel *Mytilus edulis*. *Dev. Comp. Immunol.* **16**, 111-122.
Prado-Alvarez, M., Flórez-Barrós, F., Méndez, J. and Fernandez-Tajes, J. (2013). Effect of okadaic acid on carpet shell clam (*Ruditapes decussatus*) haemocytes by *in vitro* exposure and harmful algal bloom simulation assays. *Cell Biol. Toxicol.* **29**, 189-197.
Pruzzo, C., Gallo, G. and Canesi, L. (2005). Persistence of vibrios in marine bivalves: the role of interactions with haemolymph components. *Environ. Microbiol.* **7**, 761-772.
Ray, M., Bhunia, A. S., Bhunia, N. S. and Ray, S. (2013). Density shift, morphological damage, lysosomal fragility and apoptosis of hemocytes of Indian molluscs exposed to pyrethroid pesticides. *Fish Shellfish Immunol.* **35**, 499-512.
Rink, J. C. (2013). Stem cell systems and regeneration in planaria. *Dev. Genes Evol.* **223**, 67-84.
Rolland, J. L., Pelletier, K., Masseret, E., Rieuvilleneuve, F., Savar, V., Santini, A., Amzil, Z. and Laabir, M. (2012). Paralytic toxins accumulation and tissue expression of α-amylase and lipase genes in the Pacific oyster Crassostrea gigas fed with the neurotoxic dinoflagellate *Alexandrium catenella*. *Mar. Drugs* **10**, 2519-2534.

Rosa, R. D., Santini, A., Fievet, J., Bulet, P., Destoumieux-Garzón, D. and Bachère, E. (2011). Big defensins, a diverse family of antimicrobial peptides that follows different patterns of expression in hemocytes of the oyster *Crassostrea gigas*. *PLoS ONE* **6**, e25594.

Rus, F., Kurucz, E., Márkus, R., Sinenko, S. A., Laurinyecz, B., Pataki, C., Gausz, J., Hegedus, Z., Udvardy, A., Hultmark, D. et al. (2006). Expression pattern of Filamin-240 in *Drosophila* blood cells. *Gene Expr. Patterns* **6**, 928-934.

Salamat, Z. and Sullivan, J. T. (2008). In vitro mitotic responses of the amebocyte-producing organ of *Biomphalaria glabrata* to extracts of *Schistosoma mansoni*. *J. Parasitol.* **94**, 1170-1173.

Schmitt, P., Rosa, R. D., Duperthuy, M., de Lorgeril, J., Bachère, E. and Destoumieux-Garzón, D. (2012). The Antimicrobial defense of the Pacific oyster, *Crassostrea gigas*. How diversity may compensate for scarcity in the regulation of resident/pathogenic microflora. *Front. Microbiol.* **3**, 160.

Sokol, N. S. and Cooley, L. (2003). *Drosophila* filamin is required for follicle cell motility during oogenesis. *Dev. Biol.* **260**, 260-272.

Sokolova, I. M., Evans, S. and Hughes, F. M. (2004). Cadmium-induced apoptosis in oyster hemocytes involves disturbance of cellular energy balance but no mitochondrial permeability transition. *J. Exp. Biol.* **207**, 3369-3380.

Sunila, I. and LaBanca, J. (2003). Apoptosis in the pathogenesis of infectious diseases of the eastern oyster *Crassostrea virginica*. *Dis. Aquat. Organ.* **56**, 163-170.

Turekian, K. K., Cochran, J. K., Kharkar, D. P., Cerrato, R. M., Vaisnys, J. R., Sanders, H. L., Grassle, J. F. and Allen, J. A. (1975). Slow growth rate of a deep-sea clam determined by 228Ra chronology. *Proc. Natl. Acad. Sci. USA* **72**, 2829-2832.

Vitale, I., Jemaà, M., Galluzzi, L., Metivier, D., Castedo, M. and Kroemer, G. (2013). Cytofluorometric assessment of cell cycle progression. *Methods Mol. Biol.* **965**, 93-120.

Vogt, G. (2012). Hidden treasures in stem cells of indeterminately growing bilaterian invertebrates. *Stem Cell Rev.* **8**, 305-317.

Wanamaker, A. D., Heinemeier, J., Scourse, J. D., Richardson, C. A., Butler, P. G., Eiríksson, J. and Knudsen, K. L. (2008). Very long-lived mollusks confirm 17th century AD tephra-based radiocarbon reservoir ages for North Icelandic shelf waters. *Radiocarbon* **50**, 399-412.

Watt, F. M. and Huck, W. T. S. (2013). Role of the extracellular matrix in regulating stem cell fate. *Nat. Rev. Mol. Cell Biol.* **14**, 467-473.

Xue, Q., Hellberg, M. E., Schey, K. L., Itoh, N., Eytan, R. I., Cooper, R. K. and La Peyre, J. F. (2010). A new lysozyme from the eastern oyster, *Crassostrea virginica*, and a possible evolutionary pathway for i-type lysozymes in bivalves from host defense to digestion. *BMC Evol. Biol.* **10**, 213.

Yao, C. L. and Somero, G. N. (2012). The impact of acute temperature stress on hemocytes of invasive and native mussels (*Mytilus galloprovincialis* and *Mytilus californianus*): DNA damage, membrane integrity, apoptosis and signaling pathways. *J. Exp. Biol.* **215**, 4267-4277.

Zhang, G., Fang, X., Guo, X., Li, L., Luo, R., Xu, F., Yang, P., Zhang, L., Wang, X., Qi, H. et al. (2012). The oyster genome reveals stress adaptation and complexity of shell formation. *Nature* **490**, 49-54.

Ziuganov, V., San Miguel, E., Neves, R. J., Longa, A., Fernández, C., Amaro, R., Beletsky, V., Popkovitch, E., Kaliuzhin, S. and Johnson, T. (2000). Life span variation of the freshwater pearl shell: a model species for testing longevity mechanisms in animals. *Ambio* **29**, 102-105.

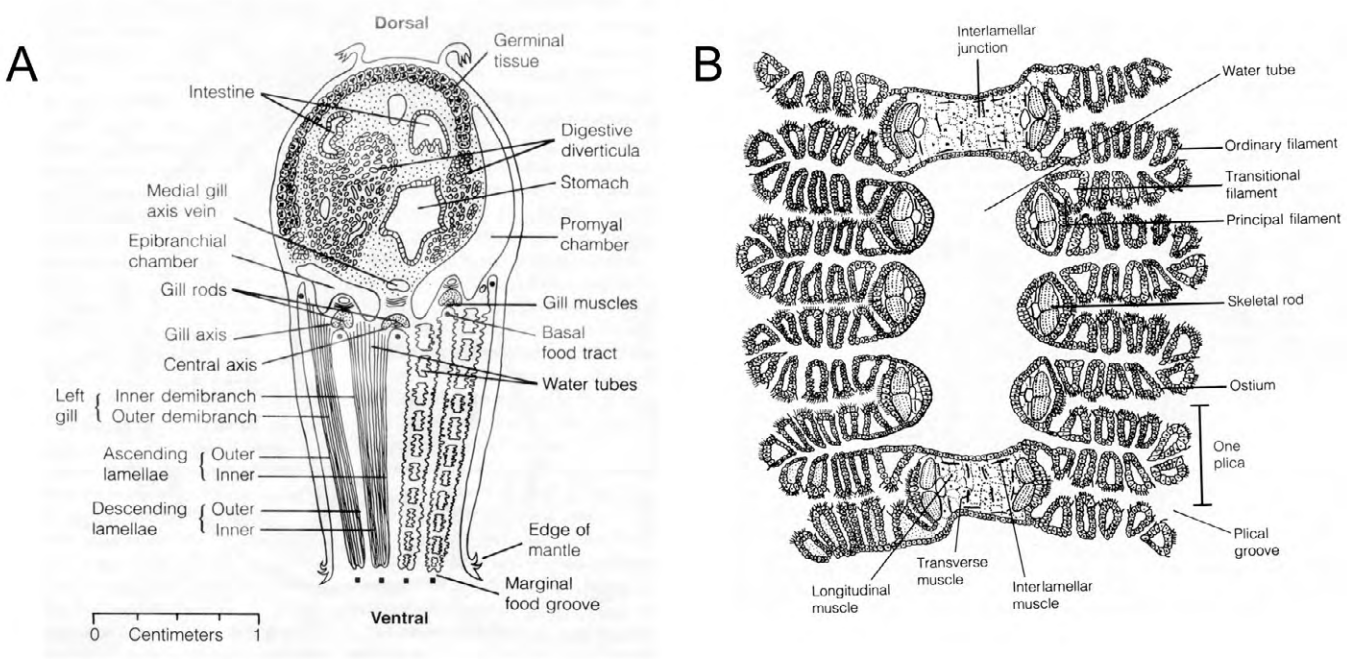

Reproduced with permission from Kennedy V, Newell R, Eble A (1996)

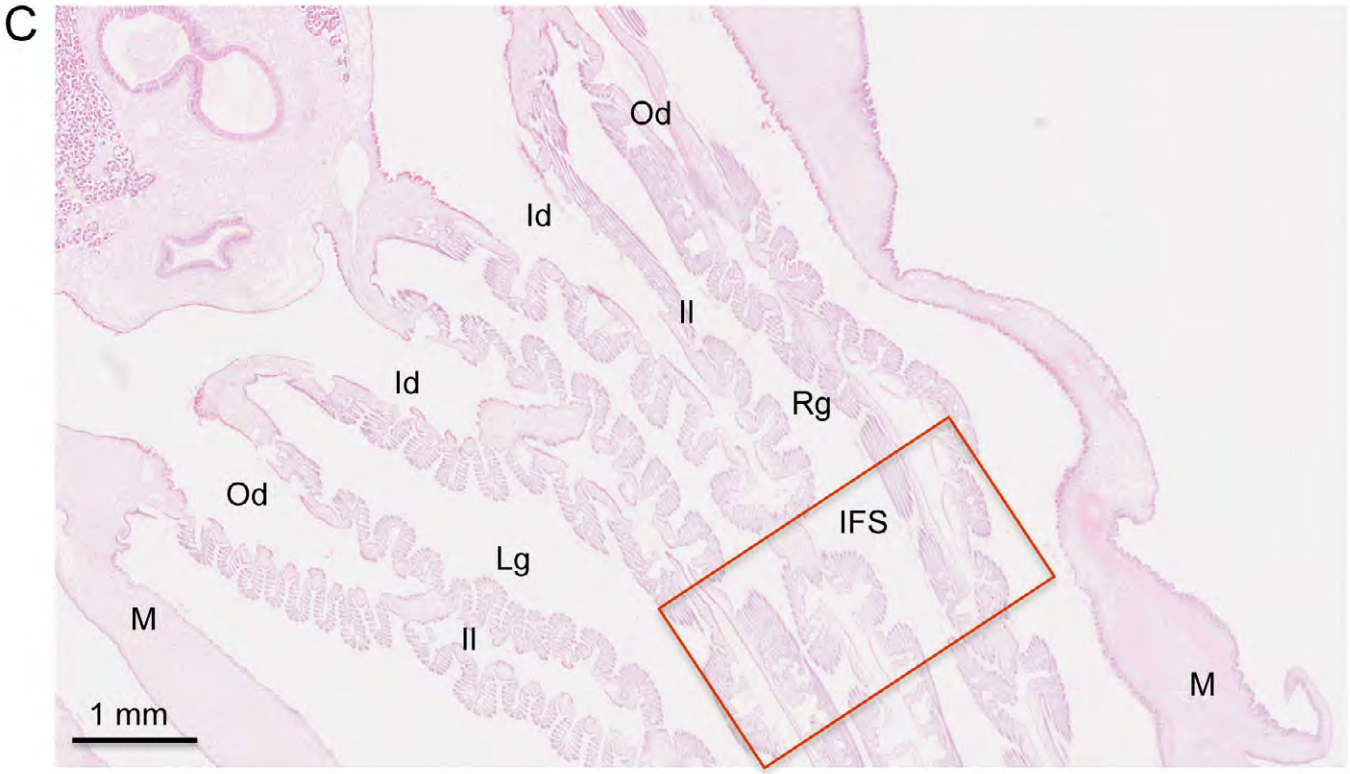

Fig. S1. General structure of the oyster gill. (A) Oyster gills are made of two V-shaped demi-branches, each composed of an ascending and a descending lamella delimiting a water tube and linked by inter-lamellar junctions. (B) Each lamella is a succession of folded structures, termed plicas, which are made of the repetition of a tubular structural unit called filament. The central part of the filament is occupied by a sinus, a space filled with hemolymph, while the basal part of the filament consists of a more or less regular layer of tightly-packed and non-ciliated cells usually referred to as epithelium. (C) Hematoxylin/eosin stained cross-section of the oyster gill and its attachment region scanned at low magnification using a Nanozoomer (Hamamatsu, Massy, France). Id, inner demi-branch; IFS, irregularly folded structure; Il, inter-lamellar junction; M, mantle; Lg, left gill; Od, outer demi-branch; Rg right gill. Credit for the drawings to Maryland Sea Grant, The American oyster *Crassotrea virginica*, editors: VS Kennedy, RIE Newell, AF Eble, Mechanisms and physiology of feeding, RIE Newell and CJ Langdon, illustrated by D Kennedy, modified from Galtsoff (1964).

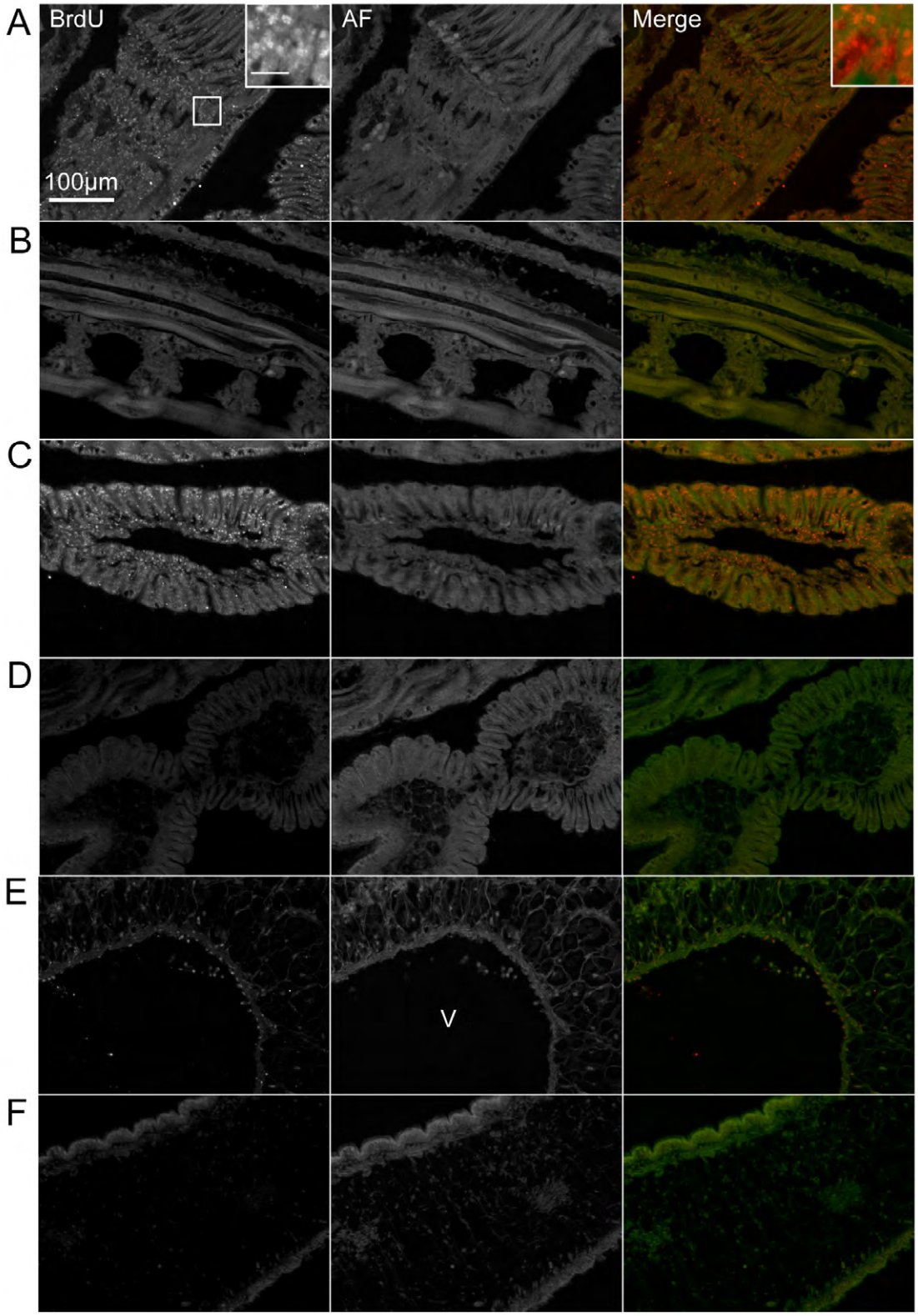

Fig. S2. Relative BrdU incorporation in the oyster gill and mantle cells. Oysters were injected with BrdU (n=3) or seawater (controls, n=3) into the sinus of the adductor muscle. The animal body was fixed in Davidson's fixative 16 hours later. Fluorescence micrographs were recorded at low magnification (x20) in the Cy3 channel for BrdU while the GFP channel is used to outline the tissues through autofluorescence (AF). Images (A,C,E) are representative of the BrdU-injected animals (n=3) and (B,D,F) of the control animals (n=3) (A) BrdU-labeling appears evenly spread in IFS section. (Inset) Intense and punctuated BrdU-labeling shown at higher magnification. Inset scale bar, 20 µm. (B) No BrdU signal on this IFS section from a control oyster injected with seawater. (C) Labeling of a region of the regularly folded gill. (D) No BrdU signal on section of the regularly folded gill from a control oyster injected with seawater. (E) BrdU labeling of a mantle area including a large vessel (V) section. A few scattered positive cells appear on the vessel vicinity. (F) No BrdU signal on this section of the mantle from a control oyster injected with seawater. V, vessel.

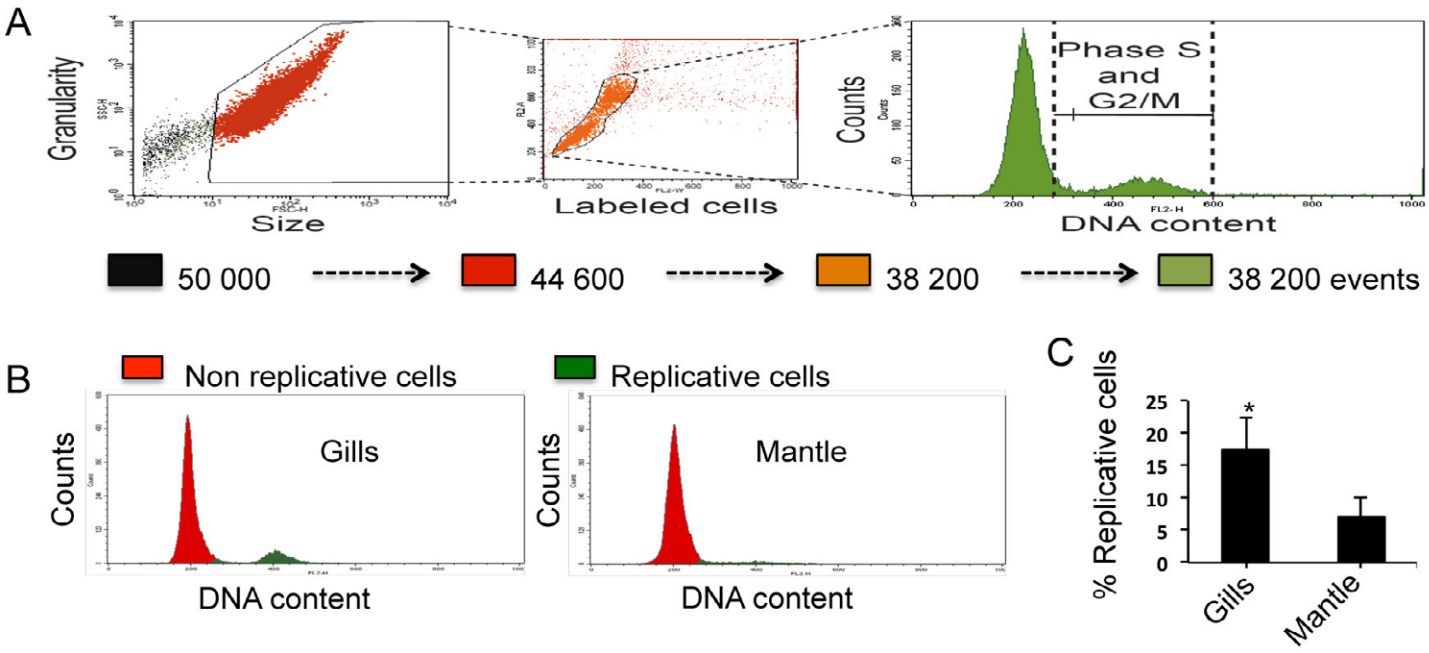

Fig. S3. **FACS analysis of the cell cycle distribution of the oyster gill and mantle cells.** Gills and mantles from oysters (n=6) were minced and digested with Pronase in Hank's buffer for dissociation into individual cells. Cells were fixed and DNA was stained with propidium iodide (PI). (A) Samples were analyzed through Flow Activated Cell Sorting. The gating procedure to isolate a population of individual cells consists in sequentially separating events. Cells were sorted through a normal light scattering to exclude bacteria and debris (granularity versus size; left panel) (50.000 to 44.600 events). Then fluorescent cells were gated according to their size in order to exclude doublets (central panel) (44.6000 to 38.200 events). Gated populations of fluorescent cells are figured according to their cell cycle profile (right panel), the peak of replicative cells corresponding to S and G2/M. (B) Cell cycle profiles for gill and mantle, which are representative of the data obtained through 5 independent experiments. Green peak, replicative cells. (C) Percentage of replicative cells in the gill and mantle cells, which are 17.3±5% and 7.2±3% for gills and mantles (n=6), respectively. Results are reported as means ± s.d. *P<0.01(two-tailed Student's t-test).

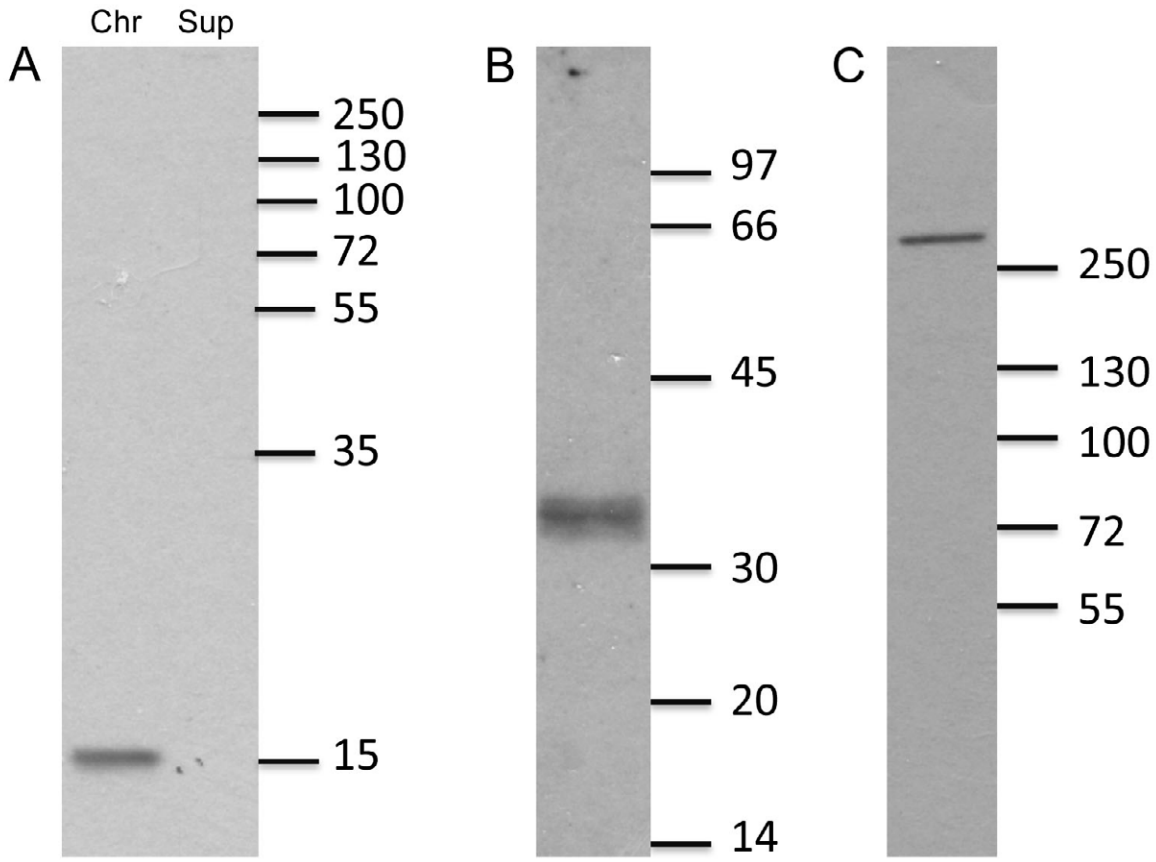

Fig. S4. Antibody specificity for oyster proteins. Immunoblots were carried out against oyster chromatin (A) or tissue extracts (B and C) (50 and 10 µg of total proteins, respectively) transferred to PVDF membrane. (A) H3P rabbit antibody revealed a unique band for histone H3 (15 kDa) on oyster chromatin extract (Chr) while no band was detected on the cytosolic extract (Sup). (B) Rabbit Sox2 antibody revealed a unique band (36 kDa) of the predicted molecular weight for Sox2 (EKC24855) on protein extract. (C) An in-house immuno-purified FLN rabbit antibody revealed a unique band migrating well over the 250 kDa marker in agreement with the predicted molecular weight for the oyster FLN (323 kDa; EKC28512).

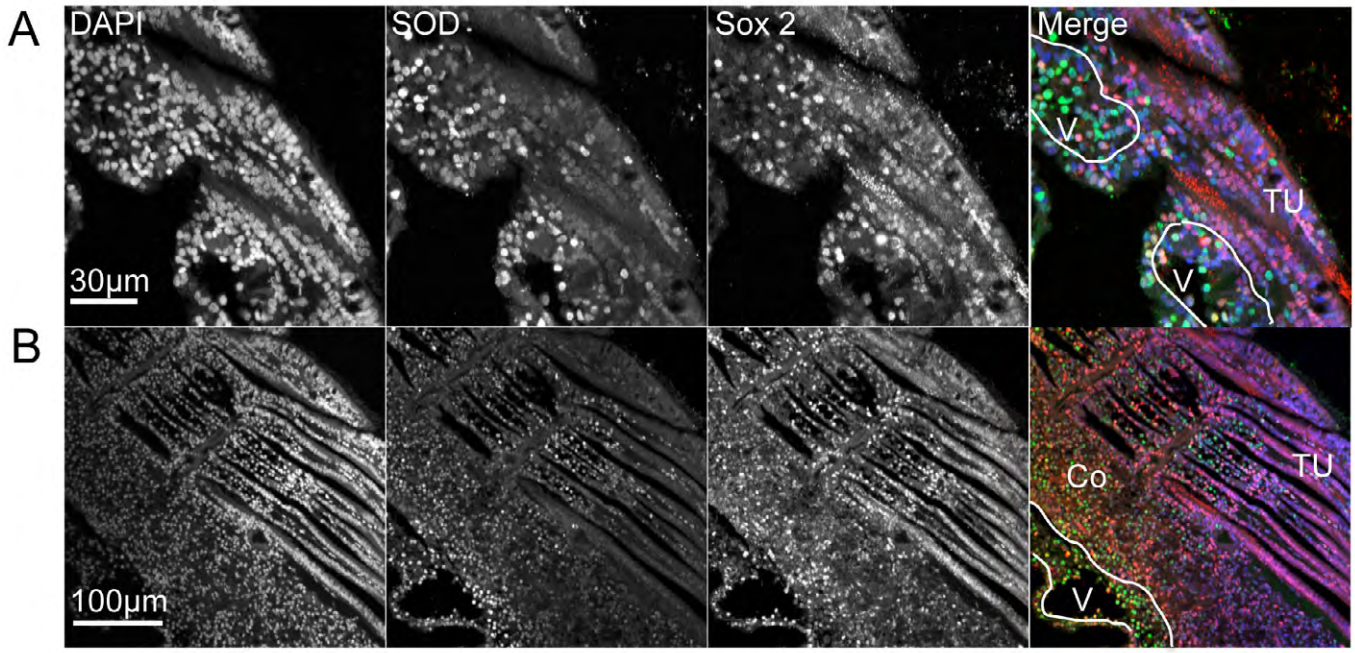

Fig. S5. **Precursor cells differentiate into hemocytes in the oyster gill.** Confocal images of the tubules (A) and convoluted structures (B) of an IFS region using Sox2 (red) and SOD (green) antibodies and DAPI (blue). Sox2-labeled cells are essentially in the tubules region while SOD-labeled cells are essentially in the underlying connective tissue (Co) and vessels (V, white outline). Cells co-labeled for Sox2 and SOD are located in the underlying connective tissue (Co) under the tubules (Tu) and in the neighboring vessel (V). Co connective tissue, V vessel, Tu tubule.

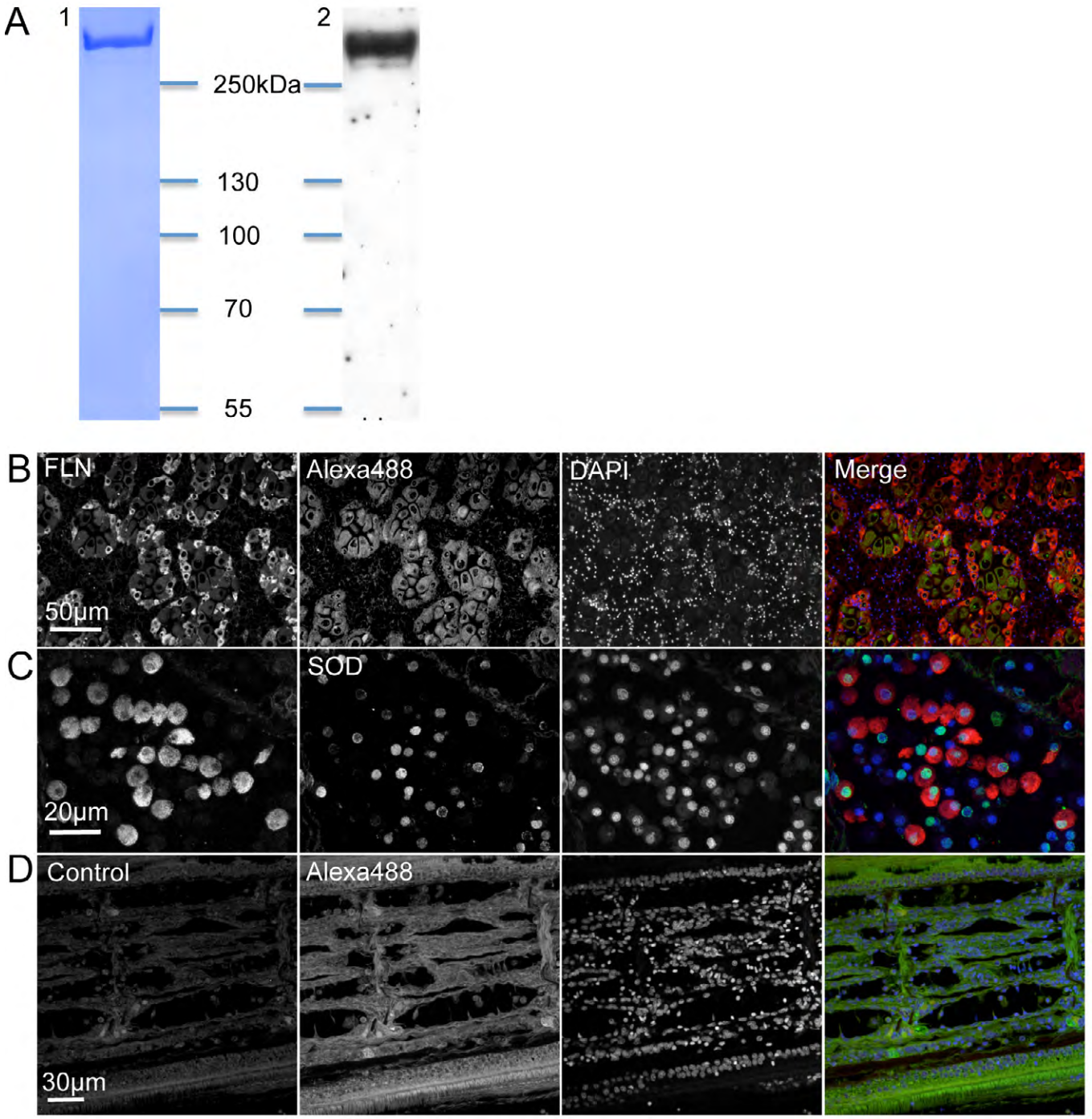

Fig. S6. **Filamin antibody specificity for a sub-population of hemocytes.** (A) Oyster FLN was purified to homogeneity on FPLC. An aliquote of a purified fraction was electrophoresed on a 7% SDS-PAGE. Colloidal Coomassie staining revealed a unique band (panel 1) migrating well above the 250 kDa marker (Thermofisher, Waltham, MA, USA). Western blot using an in-house immuno-purified rabbit FLN antibody (FLNAb) revealed a unique band (panel 2) corresponding to the Coomassie stained band. (B) Oyster cross-section encompassing the gonad submitted to IHC using FLNAb (red) and DAPI (blue). Axillary cells surrounding the oocytes were specifically and intensely labeled for FLN. Autofluorescence (Alexa 488) to outline the tissue structures. (C) Tissue sections stained using the FLN (red) and SOD antibody (green) and DAPI (blue). Image on confocal microscopy of hemocytes in a gill vessel. FLN (red) strongly stained the cytoplasm of a sub-population of hemocytes also stained for SOD (green). (D) Confocal image of a tissue section treated as in B and C but with no primary antibodies.

Table S1. FACS analysis of the DNA content of oyster gill and mantle cells.

Download Table S1

Table S2. Counting of the H3P-positive nuclei on representative regions of the mantle.

Download Table S2

Table S3. Counting of the H3P-positive nuclei on representative regions of the gill.

Download Table S3

Table S4. MS/MS data interpretation. The peak list has been searched against a UniProtKB/Swiss-Prot database of *Crassostrea gigas* combined target-decoy database (created 2013-07-30, containing 26945 target sequences plus the same number of reversed decoy sequences) using Mascot (version 2.4.1, Matrix Science, London, UK). The database contained sequences of human proteins including common contaminants (human keratins and porcine trypsin) and was created using an in-house database generation toolbox (http://msda.u-strasbg.fr). This analysis unambiguously identifies the purified protein as the oyster FLN.

Download Table S4